

OREGON STATE UNIVERSITY



DESIGN BUILD FLY 2020 - 2021

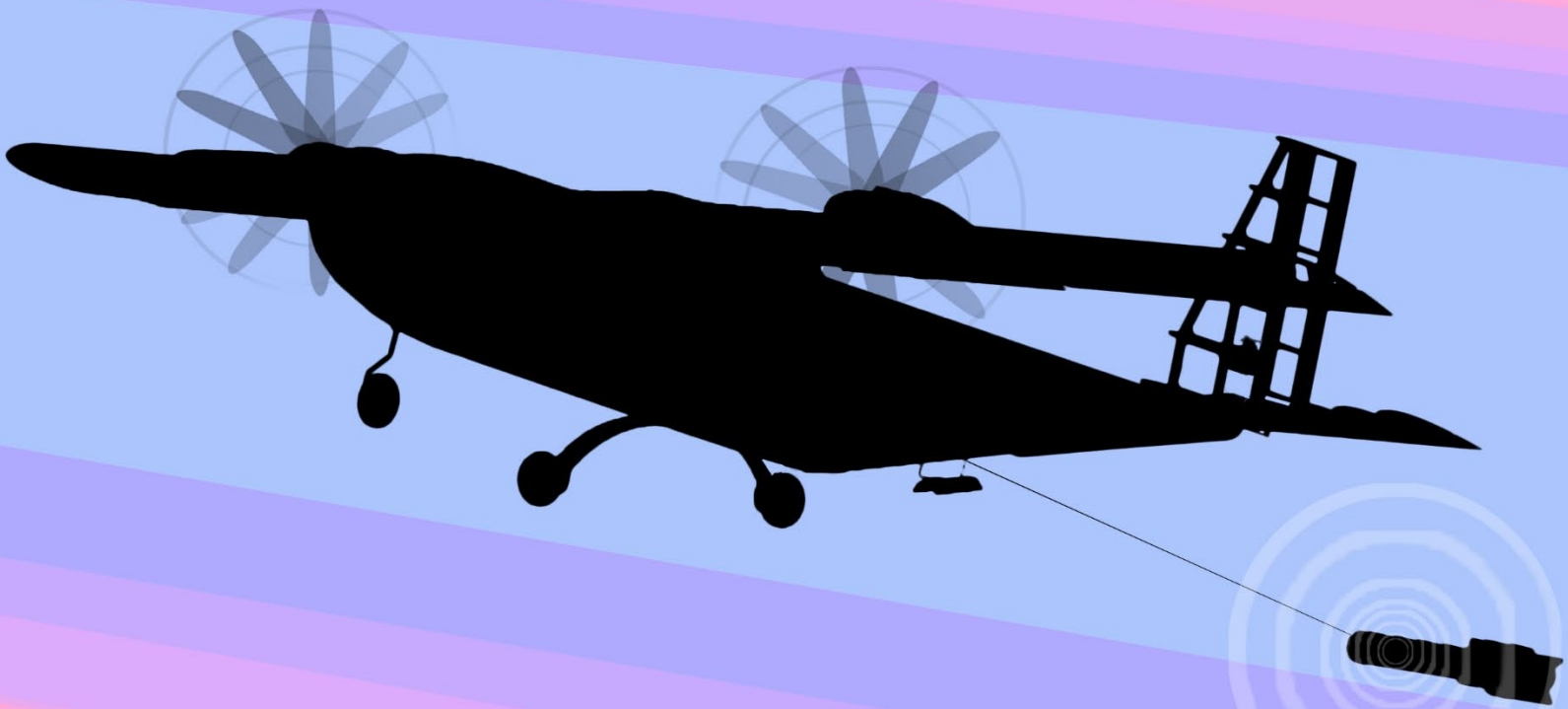




Table of Contents

| | |
|---|----|
| List of Figures | 2 |
| List of Tables | 3 |
| Acronyms and Nomenclature | 4 |
| 1 Executive Summary..... | 5 |
| 2 Management Summary | 6 |
| 2.1 Team Organization..... | 6 |
| 2.2 Project Timeline and Milestones | 7 |
| 2.3 Coordinate convention | 7 |
| 3 Conceptual Design Approach..... | 8 |
| 3.1 Mission Design Requirements..... | 8 |
| 3.2 Scoring Analysis..... | 10 |
| 3.3 Configuration Selection | 11 |
| 4 Preliminary Design..... | 17 |
| 4.1 Design Methodology..... | 17 |
| 4.2 Mission Capabilities..... | 18 |
| 4.3 Aerodynamic Qualities | 18 |
| 5 Detail Design | 28 |
| 5.1 Work Breakdown Structure | 28 |
| 5.2 Dimensional Parameters Table | 29 |
| 5.3 Structural Characteristics | 29 |
| 5.4 System Selection and Integration | 30 |
| 5.5 Weight and Balance | 34 |
| 5.6 Flight Performance Parameters | 35 |
| 5.7 Drawing Package | 35 |
| 6 Manufacturing Plan..... | 40 |
| 6.1 Manufacturing Materials | 40 |
| 6.2 Manufacturing Processes..... | 41 |
| 6.3 Manufacturing Milestones | 41 |
| 7 Component Testing and Validation | 42 |
| 7.1 Sub Team Testing | 42 |
| 7.2 Pre-Flight Checklists | 44 |
| 7.3 Flight Testing Plan..... | 45 |
| 8 Performance Results | 46 |
| 8.1 Aerodynamics and Structures Performance Results | 46 |
| 8.2 Payload Performance Results..... | 47 |
| 8.3 Propulsion Performance Results..... | 47 |
| 8.4 Flight Testing Outcomes | 50 |
| 9 Bibliography – All | 52 |



List of Figures

| | |
|---|----|
| Figure 1: Final Aircraft Design. | 5 |
| Figure 2: Team Organization Chart. | 6 |
| Figure 3: Team Project Schedule. | 7 |
| Figure 4: Aircraft Coordinate Convention. | 7 |
| Figure 5: Mission Flight Path. | 8 |
| Figure 6: Impact of Design Variables and M3 Aircraft Speed on Overall Score from Scoring Simulation. | 10 |
| Figure 7: Final Aircraft Configuration. | 16 |
| Figure 8: Propulsion Design Process Flowchart. | 17 |
| Figure 9: Flight Envelope of Aircraft. | 18 |
| Figure 10: SG6040 Lift and Drag Polar Plots. | 18 |
| Figure 11: SG6040 Airfoil Plot. | 19 |
| Figure 12: CL , Velocity, and Wing Loading Plot. | 19 |
| Figure 13: Sensor array in fuselage. | 20 |
| Figure 14: Component Drag Breakdown at $CL = 0.31$ | 22 |
| Figure 15: Drag Polar of Complete Aircraft for Each Mission. | 22 |
| Figure 16: Thrust Output Versus Motor RPM using Equation 12. | 23 |
| Figure 17: Maximum Thrust Produced for Each Propeller Diameter as A Function of Pitch. | 24 |
| Figure 18: Bomb Bay Door Servo Configuration. | 25 |
| Figure 19: Sensor Electronics Schematic. | 26 |
| Figure 20: Simulation of CP vs Fin Sizing. | 27 |
| Figure 21: Loading Paths on Fuselage. | 30 |
| Figure 22: Wing Integration with Fuselage. | 31 |
| Figure 23: Deployment and Retraction Winch. | 32 |
| Figure 24: Section View of Winch Mechanism. | 32 |
| Figure 25: Sensor Module System. | 32 |
| Figure 26: Loading Path on Sensor When Deployed. | 32 |
| Figure 27: Shipping Container Spacer. | 33 |
| Figure 28: Shipping Container Arrays in Fuselage. | 33 |
| Figure 29: Color-Coded Receiver Channels. | 34 |
| Figure 30: Transmitter Switch and Control Layout. | 34 |
| Figure 31: Prototype Aircraft Made from Foam. | 40 |
| Figure 32: Half-Span Lift Distribution. | 43 |
| Figure 33: Wing Loading Testing Setup. | 43 |
| Figure 34: Deployment and Retraction Testing at Wind Tunnel. | 44 |
| Figure 35: Competition Motor on Thrust Stand. | 44 |
| Figure 36: Wing Loaded to $n = 5$ g. | 46 |
| Figure 37: Wing load testing deflection results. | 46 |
| Figure 38: Battery Endurance Testing Results. | 48 |



| | |
|---|----|
| Figure 39: Thrust Vs Current of Different Propeller Dimensions on Static Thrust Stand. | 48 |
| Figure 40: FLIR Image of Turnigy Motor After 12-Minute Thermal Stress Test. | 49 |
| Figure 41: Flight Path of Aircraft Recorded During A M1 Simulation. | 51 |
| Figure 42: First Composite Fuselage Aircraft Prototype. | 51 |

List of Tables

| | |
|--|----|
| Table 1: Aircraft Performance Parameters. | 5 |
| Table 2: Overall Aircraft Configuration Figure of Merit Analysis. | 11 |
| Table 3: Fuselage Materials Figure of Merit Analysis. | 12 |
| Table 4: Wing Materials Figure of Merit Analysis. | 12 |
| Table 5: Wing Placement Figure of Merit Analysis. | 13 |
| Table 6: Landing Gear Configuration Figure of Merit Analysis. | 13 |
| Table 7: Empennage Configuration Figure of Merit Analysis. | 14 |
| Table 8: Propulsion Configuration Figure of Merit Analysis. | 14 |
| Table 9: Sensor Body Configuration Figure of Merit Analysis. | 15 |
| Table 10: Winch Configuration Figure of Merit Analysis. | 15 |
| Table 11: Shipping Container Configuration Figure of Merit Analysis. | 16 |
| Table 12: Theoretical TD and TW Ratios from Projected Weight and Drag. | 17 |
| Table 13: Chord Sizing Results. | 20 |
| Table 14: Component Drag Normalized to Wing Area at $CL = 0.31$ | 22 |
| Table 15: Total Stored Battery Energy Comparison. | 23 |
| Table 16: Motor Selection Figure of Merit Analysis. | 24 |
| Table 17: Final Design Dimensional Parameters and Specifications. | 29 |
| Table 18: Weight and Balance for All Flight Missions. | 35 |
| Table 19: Flight Mission Performance Parameters. | 35 |
| Table 20: Manufacturing Milestones Schedule. | 41 |
| Table 21: Test Schedule 2020-2021. | 42 |
| Table 22: Distribution of Load on Wing During Testing. | 43 |
| Table 23: Pre-Flight Checklist. | 45 |
| Table 24: Sensor Drop Testing Results. | 47 |
| Table 25: Wind Tunnel Sensor Retraction Testing Results. | 47 |
| Table 26: Predicted Versus Actual Flight Performance During Flight Testing. | 49 |



Acronyms and Nomenclature

| | | | |
|---------------------------------|--|--------------|------------------------------------|
| AIAA | American Institute of Aeronautics and Astronautics | M_2 | Mission 2 |
| AC | Aerodynamic Center | M_3 | Mission 3 |
| α, AOA | Angle of Attack | MAC | Mean Aerodynamic Chord |
| AR | Aspect Ratio | MTOW | Maximum Takeoff Weight |
| b | Wingspan | n | Load Factor |
| c | Wing Cord | N | Number of Sensors |
| CAD | Computer Aided Design | NiCad | Nickel Cadmium |
| C_D | Coefficient of Drag | NiMH | Nickel-Metal Hydride |
| $C_{D,0}$ | Zero-Lift Drag Coefficient | OSU | Oregon State University |
| CF | Carbon Fiber | P | Propeller Pitch |
| CG | Center of Gravity | PLA | Polylactic Acid |
| C_L | Coefficient of Lift | R | Turn Radius |
| $C_{L,max}$ | Maximum Coefficient of Lift | RC | Remote Control |
| C_P | Center of Pressure | Re | Reynolds Number |
| d | Propeller Diameter | RPM | Revolutions Per Minute |
| D | Drag | S | Wing Area |
| DBF | Design Build Fly | S_{ref} | Area Reference |
| DC | Direct Current | T | Thrust |
| e | Oswald Efficiency Factor | T/D | Thrust to Drag Ratio |
| ESC | Electronic Speed Controller | T/W | Thrust to Weight Ratio |
| FoM | Figure of Merit | U | Free-Stream Velocity of Air |
| FRP | Fiber-Reinforced Polymer | UAV | Unmanned Aerial Vehicle |
| g | Acceleration due to gravity | V | Velocity |
| GPS | Global Positioning System | V_{stall} | Stall Velocity |
| GM | Ground Mission | W | Aircraft Weight |
| h | Height | WBS | Work Breakdown Structure |
| Kv | RPM per Volt | λ | Taper Ratio |
| L | Lift | ρ | Density of Air |
| l | Length | ω | Angular Velocity of Propeller |
| L/D | Lift to Drag Ratio | Wh | Watt Hours |
| LiPo | Lithium Polymer | v_{ht} | Horizontal Tail Volume Coefficient |
| M_1 | Mission 1 | v_{vt} | Vertical Tail Volume Coefficient |



1 Executive Summary

The 2020-2021 American Institute of Aeronautics and Astronautics (AIAA) Design/Build/Fly (DBF) competition is designed to simulate unmanned air vehicle (UAV) operations. The specified task is to design, manufacture, and fly a remote-control aircraft that can tow a sensor for surveillance operations and transporting sensors inside of simulated shipping containers. The aircraft must complete three flight missions and complete one ground mission (GM). The flight missions will require that the aircraft takeoff in 100 ft with a maximum wingspan of 5 ft. The aircraft must also deploy, illuminate, fly, and retract a sensor that has a minimum diameter of 1 in. and minimum length to diameter ratio of 4:1. This design report details the team organization and management, aircraft and sensor design process, manufacturing and testing of the Oregon State University (OSU) *Castor Volant* aircraft shown in Figure 1 below while Table 1 provides the performance parameters.

Mission 1 (M_1) involves the aircraft completing three course laps within a time window of 5 minutes. For mission 2 (M_2), the aircraft is fully loaded with the sensor payload and must complete three laps in 5 minutes. Mission 3 (M_3) requires the deployment of a sensor midflight, towing the sensor, and retraction of the sensor, completing as many laps as possible within a 10-minute time window. The ground mission encompasses a timed integration of the payload and demonstration of flight controls. Mission scores are summed and multiplied by the report score for the total competition score. Using sensitivity analysis, the length, weight, and number of sensors was determined to be crucial to the competition score. The sensor parameters were selected, and the aircraft designed around the payload.

A large payload requires the payload carrying capabilities of a conventional aircraft configuration. An Aramid fuselage was selected to achieve structural integrity while maintaining as much space as possible inside the fuselage for payload. Balsa ribs overlaid with monokote for the wing provides good strength at a low weight. A high wing aircraft configuration coupled with tricycle landing gear offers good stability for the aircraft on the ground and in the air, which is important with the large payload. For ease of manufacturing and integration, the aircraft has a conventional empennage. Because of the large payload carried for mission 2, a twin tractor prop configuration was selected to achieve the required thrust. The sensor is a blunt nose, rocket shape because this maximizes the sensor length score and provides sufficient drag on the sensor to keep it behind the aircraft during flight. The sensor deployment and retraction are accomplished with a geared direct current (DC) motor for speed and torque. Fitted shipping containers provide the best protection for the sensor while reducing size.

Table 1: Aircraft Performance Parameters.

| Parameter | Values |
|-------------------------------|------------|
| Empty Weight (lb.) | 7.72 |
| Wingspan (in.) | 60.0 |
| Mission 1 Cruise Speed (ft/s) | 134.9 |
| Mission 2 Payload | 14 Sensors |
| Sensor Diameter (in.) | 1.0 |
| Sensor Length (in.) | 8.5 |
| Tow Line Length (in.) | 85.0 |
| $C_{L,max}$ | 1.3 |

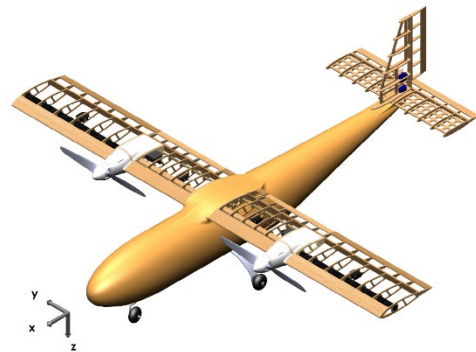


Figure 1: Final Aircraft Design.



2 Management Summary

2.1 Team Organization

The OSU AIAA DBF team is entirely managed by students, including a team lead, a deputy team lead, sub team leads and a chief editor for reporting. The team is comprised of three sub teams: Aerodynamics and Structures, Payload, and Propulsion and Controls. The competition also serves as a senior capstone design course with course deliverables that promote project management and professional engineering practices. The organization chart, shown in Figure 2, shows the support by a technical faculty advisor and the capstone class instructor. The project team leads supervise the design process and serve as the main point of contact for the team with the pilot, faculty advisor, and class instructor.

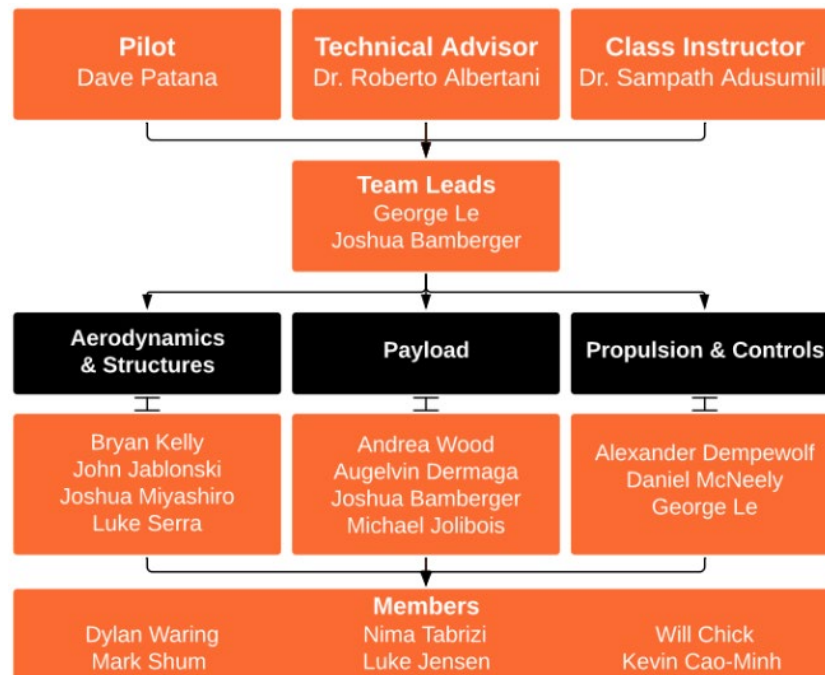


Figure 2: Team Organization Chart.

Aerodynamics and Structures: The Aerodynamics and Structures sub team is responsible for the general configuration and design of the aircraft. This includes aircraft structure, aerodynamics, control surfaces, and landing gear. Members of this sub team will manage the mass properties and longitudinal center of gravity (CG) location of the aircraft.

Payload: The Payload sub team is responsible for optimizing the aircraft's payload carrying capacity and payload functionality based on the three missions. Main sub team duties include payload aerodynamics and flight qualities, electronics, deployment, and recovery.

Propulsions and Controls: The Propulsion and Controls sub team is responsible for the design of the aircraft propulsion system, to efficiently generate enough power to fly and provide the optimal propeller, motor, and battery configuration in function of the three required missions. Each member of the propulsion sub team will



provide expertise in remote control (RC) electronic configurations and electric power management to ensure peak performance during the competition with the lowest possible system mass.

2.2 Project Timeline and Milestones

Members of the OSU DBF team consist of full-time university students, as such it was imperative to maintain effective time-management to ensure a competitive aircraft was completed by the competition date. At the beginning of the academic year, the project schedule shown in Figure 3 below was developed to track deadlines and project progress. Milestones include competition deliverables, design freeze, and competition date.

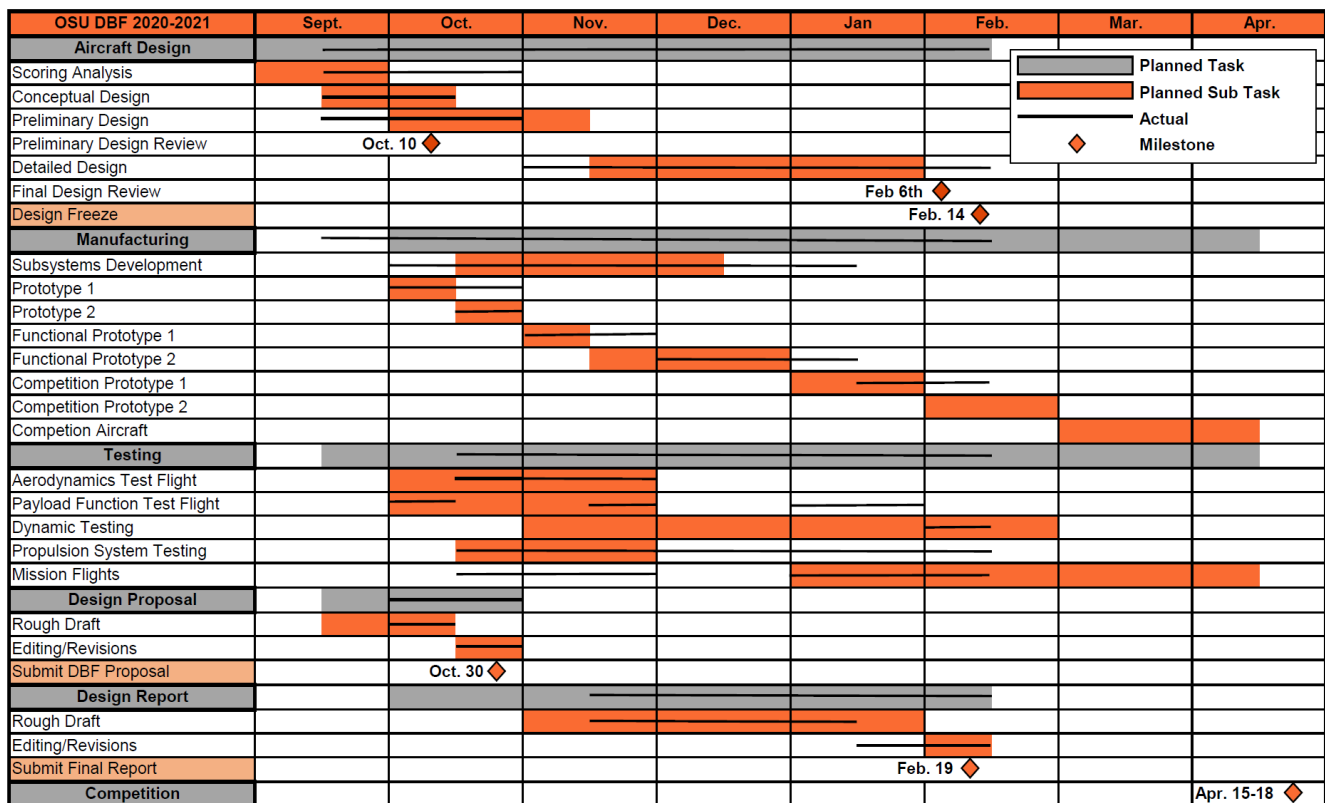


Figure 3: Team Project Schedule.

2.3 Coordinate Convention

During the initial design phase, a coordinate convention was defined to aid in design and communication shown in Figure 4 to the right. The convention was adopted from the AIAA standard, where the positive X-axis points positively through the nose of the aircraft, the Y-Axis points perpendicularly to the right of the X-axis, and the Z-axis points down through the bottom of the aircraft [1]. Additionally, the aircraft's Y-Z datum plane is located 12 in. forward of the nosecone to allow for design changes that would otherwise move the coordinate axis.

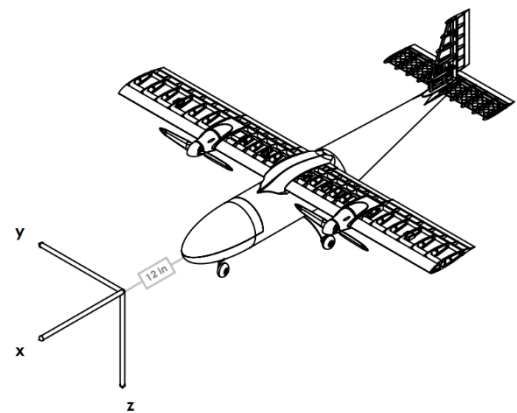


Figure 4: Aircraft Coordinate Convention.



3 Conceptual Design Approach

Scoring analysis was performed on several different designs applying the formulas outlined in the DBF competition rules. This analysis informed the best scoring design decisions for initial aircraft and sensor configurations. Once initial conceptual design parameters were determined, a refined analysis of designs commenced to converge on the final design configuration.

3.1 Mission Design Requirements

The competition consists of three flight missions and a ground mission. Takeoff for each of the three flight missions must be completed within 100 ft. of the start line. After each flight mission, a successful landing must be completed for a score to count for that mission. The lap configuration for the flight missions is shown in Figure 5 to the right. The three missions are detailed in the following sections along with the scoring for each mission.

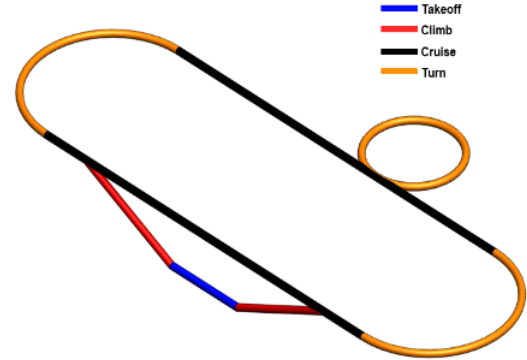


Figure 5: Mission Flight Path.

3.1.1 Mission 1 (M_1)

Mission 1 involves the aircraft performing three laps of the flight path. The flight must be completed within a 5 min. time window. The aircraft will be empty for this mission. This mission requires the aircraft to be fully functional and controlled. The scoring is shown in Equation 1 below.

$$M_1 = 1.0 \text{ for a successful mission} \quad (1)$$

3.1.2 Mission 2 (M_2)

The second flight mission requires the aircraft to be fully loaded with the sensor shipping container simulators, the sensor deployment and recovery mechanism, and the sensor within its shipping container. The score for this mission is a function of the number of sensors carried divided by the time to complete the mission from the competition teams. This value will be divided by the greatest overall number of shipping containers carried and mission time as seen in Equation 2 below.

$$M_2 = 1 + \frac{N_{\text{containers}}/time}{Max_{\text{containers}}/time} \quad (2)$$

3.1.3 Mission 3 (M_3)

For the third flight mission, the aircraft will be loaded with the sensor deployment and recovery mechanism. The sensor will be deployed during the flight. The mission time limit is 10 minutes. The score consists of the number of laps completed, the sensor length, and the sensor weight. This is divided by the best overall value from the competition teams. Equation 3 below shows how the score is calculated for M_3 . This mission is an endurance mission testing that the aircraft can complete a flight of at least 10 minutes. This mission also tests the sensor deployment, flight, and retrieval.

$$M_3 = 2 + \frac{N_{\text{laps}} * \text{sensor length} * \text{sensor weight}}{Max_{\text{laps}} * \text{sensor length} * \text{sensor weight}} \quad (3)$$



3.1.4 Ground Mission (GM)

The ground mission involves a drop test of the sensor in the shipping container, integration, and removal of the M_2 payload, integration of the deployment and retrieval mechanism, and demonstration of flight control operation. The M_2 payload will be installed in the aircraft and the flight control demonstrated to show that the payload does not interfere with the controls. The sensor will also be deployed to demonstrate proper deployment. The GM ensures the aircraft and sensor have been designed to effectively compete in the competition with optimal performance. The minimum time a team needs to complete the GM will be divided by the time for a specific team to complete the GM as is shown in Equation 4 below.

$$M_G = \frac{Min_time}{N_time} \quad (4)$$

3.1.5 Mission Score

The competition score is the sum of the flight and the ground missions. This is multiplied by the score received from the report.

$$Total\ mission\ score = M_1 + M_2 + M_3 + M_G \quad (5)$$

$$Total\ mission\ score = Total\ mission\ score * report\ score \quad (6)$$

3.1.6 Subsystem Requirements

In addition to the mission requirements seen in Section 3.1.1 to 3.1.5, the individual aircraft subsystems have requirements to abide by:

Aerodynamics and Structures

- The wingspan cannot exceed 5 ft.

Payload

- The sensor diameter must be a minimum of 1.00 in.
- The length to diameter ratio must be 4:1.
- An optional second transmitter may only be used for the deployment, operation, and recovery of the towed sensor.
- The sensor must have a minimum of three external lights visible during flight while in the deployment position.
- The sensor lights must be turned on individually, with a physical connection by towline to the aircraft.
- The sensor's power supply must be a separate entity.
- The sensor deployment and recovery system must be inside the aircraft.
- The sensor tow line must span a minimum of 10 times the total length of the sensor.
- The sensor shipping container must fully cover the sensor and protect the sensor during drop tests.
- All shipping containers and shipping container simulators must be the same size.



Propulsion and Controls

- Only Nickel Cadmium (NiCad)/Nickel-Metal Hydride (NiMH) or Lithium Polymer (LiPo) battery packs may be picked for the propulsion package.
- Individual LiPo battery packs must not exceed 100 watt-hours (Wh), with a 200 Wh maximum total stored energy.
- NiCad/NiMH battery packs must be clearly labeled specifying cell chemistry.
- All battery packs may not be altered from the original product release.
- An external ON/OFF switch must be present on the aircraft.
- A proper Fail-Safe must be programmed into the transmitter for the control system.

Takeoff

- The aircraft has maximum distance of 100 ft. before takeoff.
- No external assistance outside of the propulsion package is allowed for the aircraft to takeoff.

3.2 Scoring Analysis

Due to the high number of independent variables and the numerous constraints, a population-based scoring simulation was selected, the output and trends of which are shown in Figure 6 below. Historical real values from previous DBF competition aircraft were used to define legitimate boundaries in the analysis. The sensitivity analysis confirmed the high impact of the sensor size, number, and weight on the mission score. Consequently, the aircraft design was based around the sensor.

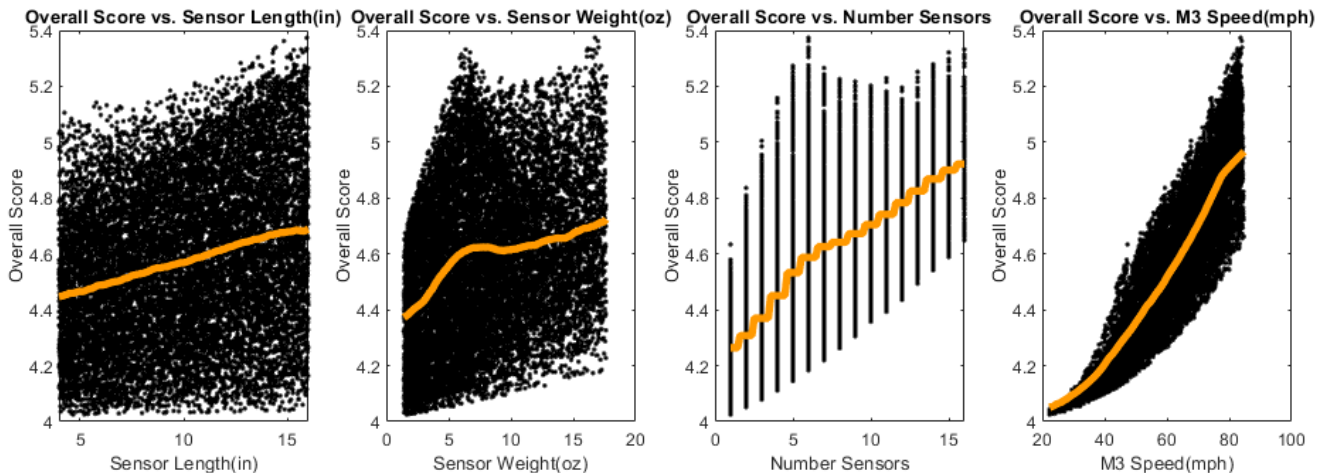


Figure 6: Impact of Design Variables and M_3 Aircraft Speed on Overall Score from Scoring Simulation.

An 8.5 in. length with a max diameter of 2.13 in. and a weight of 0.44 lbs. were the sensor parameters that yielded the highest score while allowing for storage of a significant number of sensors in the fuselage. Given the sensor weight and aircraft empty weight from historical data, the aircraft maximum takeoff weight ($MTOW$) was estimated to be 18.1 lbs. with reasonable thrust requirements from a twin propeller configuration. The dimensions and the number of sensors, 14, resulted in an estimated fuselage volume of 610.5 in.³.




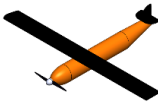


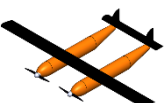
3.3 Configuration Selection

To determine an aircraft configuration to best meet the mission requirements, numerous design alternatives were compared using weighted decision matrices. Selections for major components of the aircraft were made using figures of merit which provided an analytical comparison between design alternatives based on their ability to meet design requirements. Alternatives were ranked by their ability to satisfy a given design requirement from worst to best on a scale from 1 to 5. Each score is multiplied by the design requirement weight based on importance.

3.3.1 Overall Aircraft Configuration

The mission requirements and scoring analysis indicated the need for a high-lift aircraft with internal volume to transport several shipping containers. As seen in Table 2, four aircraft configurations were considered: conventional, flying wing, tandem wing, and twin fuselage. The conventional configuration provides good payload capacity and is simple to manufacture. The flying wing has the lowest drag due to a reduction in interference drag. As a result, this configuration can achieve higher speeds. The flying wing, however, has significantly lower payload capacity and is difficult to manufacture. A tandem wing configuration provides increased lift to carry a heavier payload but has a longer manufacturing time and lower stability. The twin fuselage provides excellent payload capacity to the detriment of manufacturability and weight.

Table 2: Overall Aircraft Configuration Figure of Merit Analysis.

|  | |  |  |  |  |
|---|-------------|---|---|---|---|
| Figure of Merit | Weighting | Conventional | Flying Wing | Tandem Wing | Twin Fuselage |
| Weight | 0.30 | 4.00 | 4.50 | 3.00 | 2.00 |
| Payload Capacity | 0.25 | 4.00 | 2.00 | 4.00 | 5.00 |
| Stability | 0.20 | 4.00 | 2.00 | 2.00 | 4.00 |
| Drag | 0.15 | 3.00 | 5.00 | 3.00 | 2.00 |
| Manufacturability | 0.10 | 5.00 | 2.00 | 3.00 | 1.00 |
| Total | 1.00 | 3.95 | 3.20 | 3.05 | 3.05 |

3.3.2 Fuselage Materials

Determination of the fuselage materials affect the structural integrity of the aircraft, the internal space, as well as the cost and ease of manufacturing. A balsa-monokote fuselage is lightweight, simple to manufacture, easy to service, and low cost. However, due to the structural requirements, the internal space is reduced without a significant increase in durability. An aramid fuselage offers superior durability and internal space with good weight savings. Aramid is costly and difficult to manufacture and service. Lastly, the foam fuselage is simple to fabricate at low cost, but severely reduces internal space. Foam is also not durable and requires a significant weight to achieve enough structural integrity to fly. Based on Table 3, the optimal fuselage material was determined to be Aramid.



Table 3: Fuselage Materials Figure of Merit Analysis

| Figure of Merit | Weighting | Balsa-Monokote | Aramid | Foam |
|---------------------|-------------|----------------|-------------|-------------|
| Weight | 0.30 | 5.00 | 4.00 | 3.00 |
| Interior Volume | 0.30 | 2.00 | 5.00 | 1.00 |
| Durability | 0.20 | 2.00 | 4.00 | 1.00 |
| Cost | 0.10 | 4.00 | 1.00 | 4.00 |
| Ease of Manufacture | 0.05 | 4.00 | 2.00 | 5.00 |
| Serviceability | 0.05 | 4.00 | 3.00 | 3.00 |
| Total | 1.00 | 3.30 | 3.85 | 2.20 |

3.3.3 Wing Materials

The construction of the wing is critical to achieving appropriate strength for wing loading while minimizing weight. The three materials different materials considered included balsa-monokote, fiberglass, and foam as shown in Table 4. A balsa-monokote wing has good strength with low cost and weight. The empty space in a balsa-monokote wing allows for ease of serviceability for components inside the wing. A fiberglass wing is the strongest option, but it is heavy and requires significant time and effort to fabricate. Service access to internal components is also limited with a fiberglass wing. A foam wing is inexpensive and straightforward to manufacture but sacrifices strength and component serviceability.

Table 4: Wing Materials Figure of Merit Analysis.

| Figure of Merit | Weighting | Balsa-Monokote | Fiberglass | Foam |
|---------------------|-------------|----------------|-------------|-------------|
| Weight | 0.40 | 5.00 | 4.00 | 4.00 |
| Strength | 0.25 | 4.00 | 5.00 | 3.00 |
| Ease of Manufacture | 0.20 | 4.00 | 1.00 | 5.00 |
| Cost | 0.10 | 5.00 | 2.00 | 5.00 |
| Serviceability | 0.05 | 4.00 | 2.00 | 2.00 |
| Total | 1.00 | 4.50 | 3.35 | 3.95 |




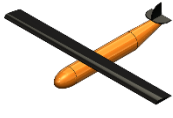
3.3.4 Wing Placement

Three different wing placement locations were considered for the aircraft: low, middle, and high in Table 5. A low wing is easily mounted on the aircraft and does not interfere with internal space for the payload. The low wing, however, has the least ground clearance. The high wing is also easily mounted to the top of the aircraft and does not interfere with the payload capacity. The high wing configuration is generally more stable and provides the



most ground clearance. Lastly, the mid wing requires complex integration as internal bracing through the fuselage is necessary which also decreases the space available for the payload.





Table 5: Wing Placement Figure of Merit Analysis.

|  | |  |  |  |
|---|-------------|---|--|---|
| Figure of Merit | Weighting | Low-Wing | Mid-Wing | High-Wing |
| Weight | 0.30 | 3.00 | 2.00 | 3.00 |
| Ground Clearance | 0.25 | 1.00 | 3.00 | 5.00 |
| Stability | 0.20 | 2.00 | 3.00 | 4.00 |
| Payload Capacity | 0.15 | 4.00 | 2.00 | 4.00 |
| Fuselage Integration | 0.10 | 4.00 | 1.00 | 4.00 |
| Total | 1.00 | 2.55 | 2.35 | 3.95 |

3.3.5 Landing Gear Configuration

Landing gear was especially important to consider due to the use of a deployable sensor. The conventional landing gear promotes good ground handling and is durable, but the rear wheel has the possibility of interference with the deployed sensor. The tricycle offers good ground handling and the least interference with the deployed sensor. It is durable with limited weight increase from the conventional configuration. The tail skid is the lightest and lowest drag configuration with one wheel being removed but does not handle well on the ground and has potential to catch the payload during deployment. As seen in Table 6 below, the tricycle configuration was determined to be the optimal landing gear design.

Table 6: Landing Gear Configuration Figure of Merit Analysis.


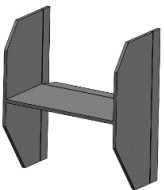


|  | |  |  |  |
|---|-------------|---|--|---|
| Figure of Merit | Weighting | Conventional | Tricycle | Tail Skid |
| Payload Compatibility | 0.35 | 2.00 | 4.00 | 1.00 |
| Weight | 0.25 | 3.00 | 3.00 | 5.00 |
| Ground Handling | 0.25 | 4.00 | 5.00 | 1.00 |
| Durability | 0.15 | 4.00 | 4.00 | 1.00 |
| Total | 1.00 | 3.05 | 4.00 | 2.00 |

3.3.6 Empennage Configuration

The empennage provides stability and control for the aircraft. Three tail configurations were considered in Table 7 below. An H-tail is the heaviest and most complex to manufacture but provides excellent yaw control for the aircraft. The conventional tail is the simplest to manufacture and most common tail design used in aviation. The T-tail induces the least drag but is difficult to integrate.




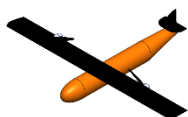
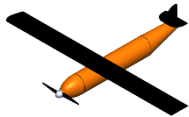
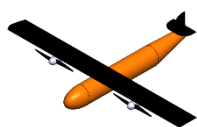
Table 7: Empennage Configuration Figure of Merit Analysis.

|  | |  |  |  |
|---|-----------|---|--|---|
| Figure of Merit | Weighting | H-Tail | Conventional | T-Tail |
| Weight | 0.40 | 2.00 | 3.00 | 3.00 |
| Stability | 0.30 | 4.00 | 3.00 | 3.00 |
| Drag | 0.20 | 4.00 | 3.00 | 3.50 |
| Simplicity | 0.10 | 1.00 | 5.00 | 2.00 |
| Total | 1.00 | 2.90 | 3.20 | 3.00 |

3.3.7 Propulsion Configuration

The propulsion system must provide sufficient thrust to carry a high payload and reach high velocities to reduce lap times. A twin pusher configuration yields the highest efficiency, due to the airflow being pulled over the wing, discouraging air separation from the wing but increases the possibility of interference with the sensor towline. The single tractor motor is the simplest to replace and repair but sacrifices thrust-to-weight (T/W) and ground clearance. The twin tractor configuration shown in Table 8, offers many of the benefits of a twin pusher but significantly decreases the potential for towline interference.

Table 8: Propulsion Configuration Figure of Merit Analysis.

|  | |  |  |  |
|---|-----------|---|--|---|
| Figure of Merit | Weighting | Twin Pusher | Single Tractor | Twin Tractor |
| Thrust to Weight | 0.30 | 5.00 | 3.00 | 4.50 |
| Cost | 0.20 | 2.00 | 3.00 | 2.00 |
| Payload Integration | 0.15 | 1.00 | 5.00 | 3.50 |
| Ground Clearance | 0.15 | 4.50 | 2.00 | 4.00 |
| Ease of Integration | 0.10 | 3.00 | 4.00 | 3.00 |
| Replaceability | 0.10 | 2.50 | 4.00 | 2.50 |
| Total | 1.00 | 3.275 | 3.35 | 3.425 |


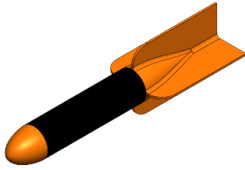
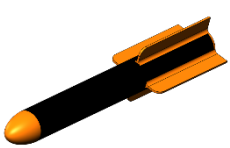
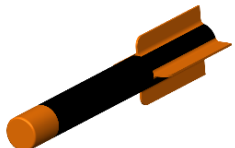
3.3.8 Sensor Body Configuration

The sensor body must be aerodynamically stable and maintain a minimum aspect ratio of 4:1. A tapered end will decrease drag and allow for more fin surface area, increasing stability in pitch and yaw. However, the taper would also reduce the length of the 1 in. diameter cross section, reducing the score. The reduced drag from the tapered end allows for forward swing of the sensor when the aircraft slows increasing the potential for a prop strike of the sensor or towline. The blunt end increases the drag and 1 in. cross section length but reduces the fin surface area. Lastly, a blunt nose and blunt end rocket produces the most drag, preventing forward swing, while



also optimizing the sensor length for the score. The blunt nosecone does increase the instability of the sensor in flight, however.



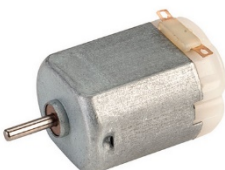

Table 9: Sensor Body Configuration Figure of Merit Analysis.

|  | |  |  |  |
|---|-----------|---|--|---|
| Figure of Merit | Weighting | Tapered End Rocket | Blunt End Rocket | Blunt Nose & End |
| Drag | 0.20 | 4.00 | 3.00 | 2.00 |
| Pitch Stability | 0.30 | 5.00 | 5.00 | 4.00 |
| Swing Stability | 0.20 | 2.00 | 3.00 | 5.00 |
| Length | 0.30 | 2.00 | 4.00 | 5.00 |
| Total | 1.00 | 3.30 | 3.90 | 4.10 |

3.3.9 Winch Configuration

The winch for deploying and retracting the sensor needs to be compact and as light-weight as possible to reduce the aircraft size and overall weight. The winch also must have the torque and speed to retract the payload before landing. The three actuation options considered in Table 10 for the winch were a geared DC motor, DC motor, and continuous servo. DC motors can achieve high RPM but are hard to control, as they cannot be directly connected to a receiver channel. A geared DC motor allows the RPM to be decreased to a usable speed for the winch and increases the torque of the motor. A servo motor has high torque for its size and does not require extra components for controllability. A servo has lower RPM than a geared DC motor which would increase the retraction time.

Table 10: Winch Configuration Figure of Merit Analysis.

|  | |  |  |  |
|---|-----------|---|--|---|
| Figure of Merit | Weighting | Geared DC Motor | DC Motor | Servo Motor |
| RPM | 0.40 | 5.00 | 4.00 | 2.00 |
| Torque | 0.20 | 5.00 | 2.00 | 3.00 |
| Weight | 0.10 | 2.00 | 2.50 | 3.00 |
| Controllability | 0.30 | 2.00 | 2.00 | 5.00 |
| Total | 1.00 | 3.80 | 2.85 | 3.20 |


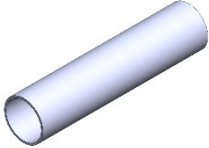
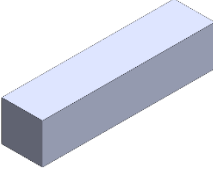
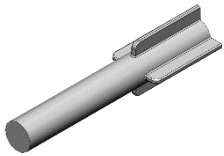
3.3.10 Shipping Container Configuration

The shipping container needs to protect the sensor from impact from a 10 in. drop. The container also needs to be able to fit and be secured inside the fuselage. The cylinder configuration requires the cross-sectional area of



the container to be at least 2.13 in. to accommodate the diameter of the sensor fins. The cylinder has a decent weight-to-size ratio and durability. The cuboid requires the most volume inside the fuselage. The corners would also concentrate stresses, meaning impacts are more likely to damage this shipping container configuration. Lastly, the fitted shipping container tightly conforms to the shape of the sensor. Given that the cross-sectional area would be only slightly larger than the sensor itself, it boasts the best area and weight score. Because the tail fins protrude from the sensor, the fitted container would also have stress concentrations when dropped on those surfaces.

Table 11: Shipping Container Configuration Figure of Merit Analysis.

|  | |  |  |  |
|---|-----------|---|--|---|
| Figure of Merit | Weighting | Cylinder | Cuboid | Fitted |
| Cross-sectional Area | 0.25 | 3.00 | 2.00 | 5.00 |
| Weight | 0.25 | 3.00 | 2.00 | 5.00 |
| Durability | 0.25 | 4.00 | 3.00 | 3.00 |
| Securement | 0.25 | 4.00 | 2.00 | 5.00 |
| Total | 1.00 | 3.50 | 2.25 | 4.50 |

3.3.11 Final Conceptual Design

Using the figures of merit and scoring analysis, the final conceptual design was selected with the optimal characteristics. A high wing aircraft with twin tractor propulsion, conventional empennage, and a tricycle landing gear configuration held the most merit for use while holding the maximum payload and towing the sensor. The aircraft configuration is shown in Figure 7.

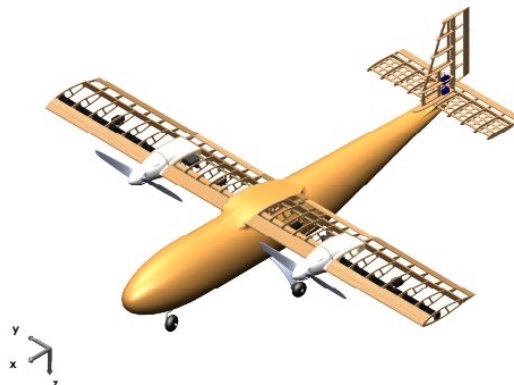


Figure 7: Final Aircraft Configuration.

3.4 Propulsion Conceptual Design

The propulsion package was established by using calculated baseline values from the scoring analysis as well as provided limitations laid out in the competition rules. The most relevant parameters that came from these sources in optimizing the propulsion system were the calculated cruise speeds, mission-specific aircraft weights and drag,



and the battery power limitations. By using varied analyses, these baseline values shaped the performance targets for the propulsion package. The process flow for characterizing the propulsion package is shown in Figure 8 below.

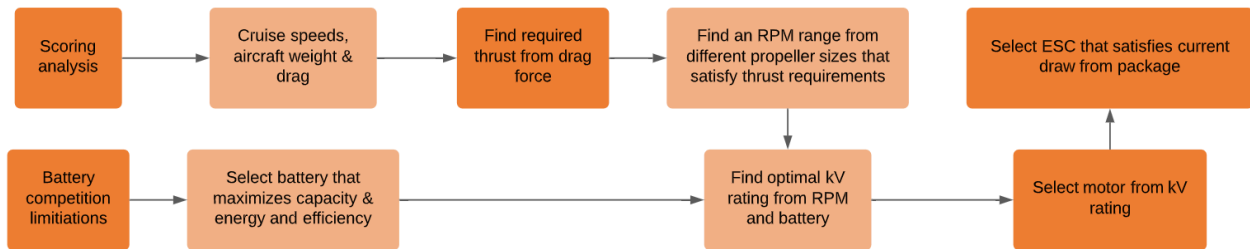


Figure 8: Propulsion Design Process Flowchart.

Once the scoring analysis provided a projected MTOW and drag for each mission, the required thrust values were found for each mission by multiplying the estimated drag force at cruise speed by a maximum thrust to drag (T/D) ratio of 1.2. During battery drop off testing, there was an approximate 14% observed drop in thrust due to voltage sag. To ensure the maximum T/D stayed above 1.0 during flight to maintain the desired cruise speed, and adding 0.06 for additional safety, a ratio of 1.2 was used. Table 12 below shows the projected MTOW, projected drag, and both T/D and T/W ratios for each mission and its resulting required thrust.

Table 12: Theoretical T/D and T/W Ratios from Projected Weight and Drag.

| Mission | Projected MTOW (lb.) | Projected Drag (lb.) | T/D Ratio (lb./lb.) | Required Thrust (lb.) | Resulting T/W Ratio (lb./lb.) |
|---------|----------------------|----------------------|-----------------------|-----------------------|---------------------------------|
| 1 | 8.82 | 2.00 | 1.20 | 2.40 | 0.27 |
| 2 | 19.84 | 2.00 | 1.20 | 2.40 | 0.12 |
| 3 | 12.13 | 2.24 | 1.20 | 2.85 | 0.24 |

A battery was selected to provide the aircraft with the most power and capacity possible while remaining under the competition limits. The required thrust and battery then informed the selection of a suitable RPM and propeller combination. From RPM values and battery voltage, a motor Kv rating could then be calculated to find a matching motor. The last component to complete the propulsion package was an electronic speed controller (ESC). This component was selected with the help of eCalc, an electric drive simulation software, for each of the missions. Inputting projected drag and weight values inside the simulator provided an estimated current draw at 100% throttle. As a safety precaution to prevent overheating, a safety factor of 30% was added on the maximum current draw to select the optimal ESC.

4 Preliminary Design

4.1 Design Methodology

The design methodology was focused on optimizing sub-systems to maximize mission scores while minimizing points of failure on the aircraft. Variables that increased mission scores such as lap time and sensor weight were used in creating initial designs. These designs were put through detailed analysis and simulation to validate that they provided the expected functionality without adding undesirable characteristics to the aircraft such as



increased weight or unneeded complexity. These designs were manufactured and tested to verify previous analyses.

4.2 Mission Capabilities

The Figure 9 below displays the flight envelope for the aircraft. Although an initial design load factor of 2.5 was chosen to pass the wing-tip test, a higher load factor of 5 was ultimately chosen to achieve a faster corner velocity, allowing for a 78.5-degree bank angle level turn for the fully loaded aircraft.

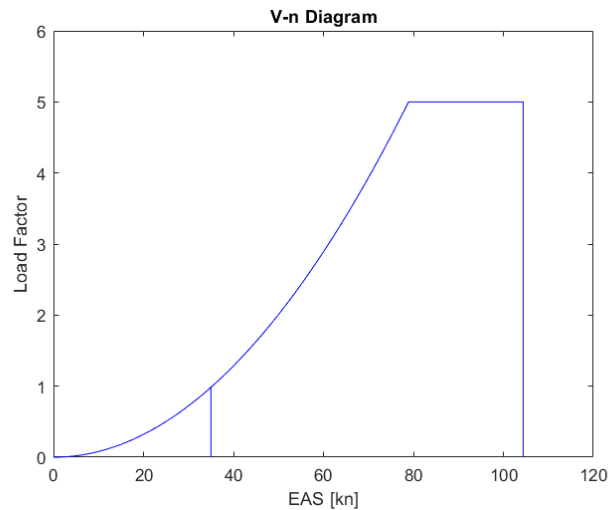


Figure 9: Flight Envelope of Aircraft.

4.3 Aerodynamic Qualities

4.3.1 Airfoil Selection

The required cruise speed and initial wing design determined the airfoil Reynold's number (Re) design range in between 400,000 and 500,000 based on the wing mean aerodynamic chord (MAC). A minimum thickness of 15% was necessary to provide sufficient interior space for electronics and an efficient structure. The selected airfoil was cross-referenced with high lift-to-drag ratio at expected cruise lift coefficients from 0.3 to 0.5.

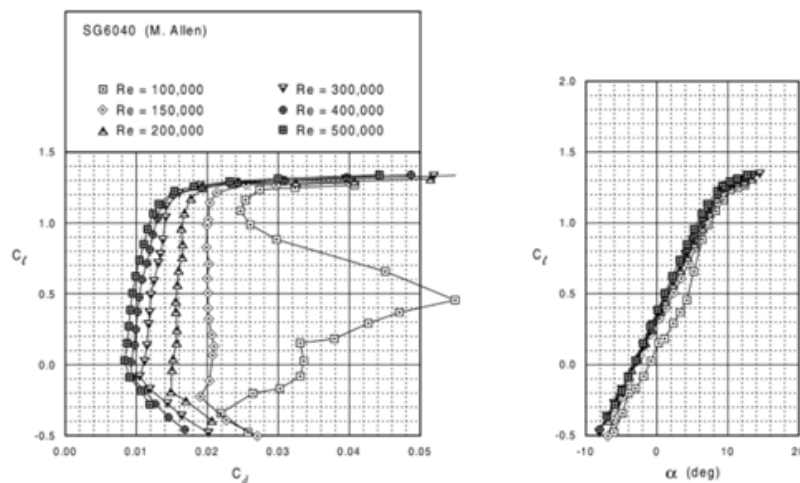


Figure 10: SG6040 Lift and Drag Polar Plots.



Experimental airfoil aerodynamic data were preferred versus pure numerical estimates. The airfoil SG6040 plotted in Figure 11 below was selected from wind tunnel data [2]. The airfoil has a camber of 16% and a max lift coefficient ($C_{L,max}$) of 1.3 at the required Reynold's numbers.

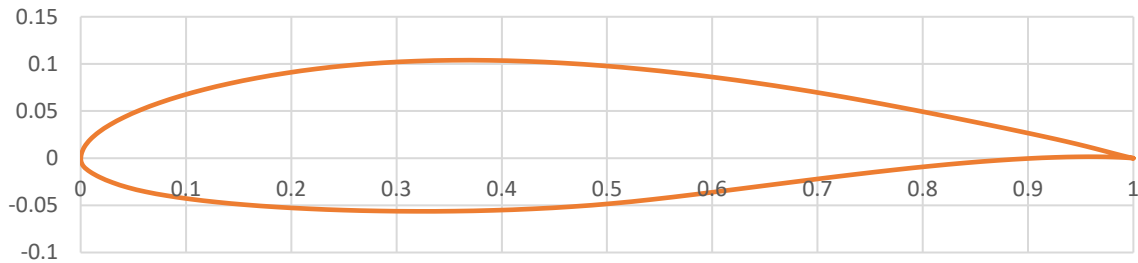


Figure 11: SG6040 Airfoil Plot.

4.3.2 Lift Performance

The design lift coefficient was selected with the primary goal to maximize speed and endurance while providing enough wing volume for an efficient structure and acceptable takeoff and landing performance. As takeoff length was not a great concern, a high wing loading value was selected for greater level speed. Using a combination of the target payload for mission two and historical data, it was determined that the max takeoff weight would be 18.10 lbs. A lift coefficient versus flight speed spreadsheet was applied to compare the lift coefficients at different wing-loading values at the target cruise speed. Using drag polar shown in Figure 12, a low cruise lift coefficient was determined to be favorable with a target cruise lift coefficient between 0.2 and 0.4.

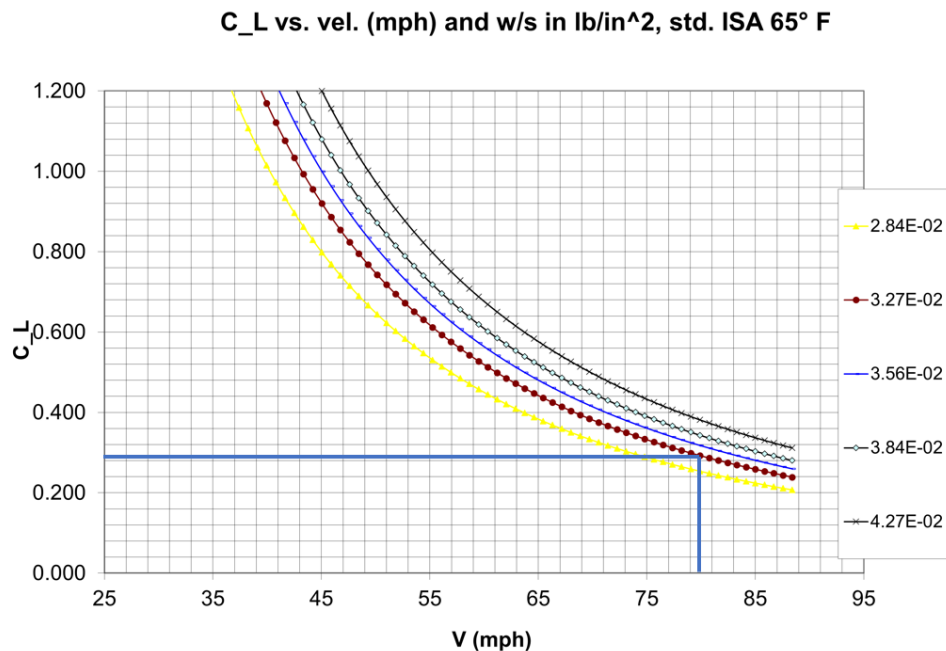


Figure 12: C_L , Velocity, and Wing Loading Plot.

While the graph confirmed the feasibility of the values obtained from the scoring analysis, it was determined that the landing speed was too great to land successfully. The chord was increased after some analysis on stall



speed (V_{stall}) summarized in Table 13, and 30% chord flaps were implemented to reach an acceptable landing speed.

Table 13: Chord Sizing Results.

| Chord (in.) | W/S (lb./ft ²) | Re (80 mph) | Re (35 mph) | AR | V_{stall} (mph) |
|-------------|----------------------------|---------------|---------------|-------------|-------------------|
| 6.92 | 0.0427 | 421000 | 180000 | 8.67 | 42 |
| 8.69 | 0.0327 | 529000 | 227000 | 6.90 | 37.6 |
| 10.27 | 0.0284 | 625000 | 268000 | 5.84 | 34.5 |

4.3.3 Fuselage Sizing and Layout

The fuselage design was driven primarily by the shipping container storage requirement. Based on the optimized sensor configuration from the scoring analysis, it was determined a large internal volume was necessary. The diameter and length of the main fuselage section was chosen based on the shipping container packing dimensions of the selected honeycomb array. The fuselage was designed with a taper in the tail section to improve aerodynamics and reduce weight. The length of the tail section and nose were determined from fineness ratios developed by Gudmundsson to minimize drag [3].

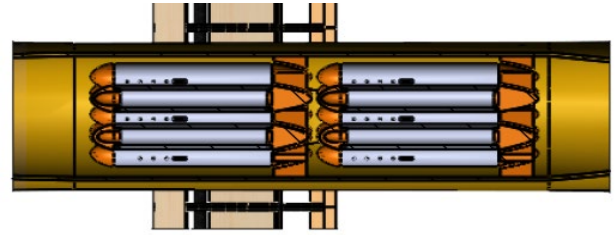


Figure 13: Sensor array in fuselage.

$$\frac{L_{tail}}{D_{fus}} = 3.00 \text{ to } 3.35, \quad \frac{L_{nose}}{D_{fus}} = 1.45 \text{ to } 1.75 \quad (7)$$

The upper bound of the tail fineness ratio was selected to minimize aerodynamic drag. A positive effect is also the increase of the tail surfaces' moment arm, decreasing the area required for each. The lower bound of the nose fineness ratio was chosen to minimize size and material weight.

4.3.4 Longitudinal Stability

Longitudinal stability is crucial for safe and controllable flight and is influenced primarily by the CG location, wing aerodynamic center, and the horizontal tail size and moment arm. For a conventional single wing and aft tail airplane configuration, it is important to locate the CG just forward of the airplane's aerodynamic center. The horizontal tail placement and size was determined through iterative calculations based on tail volume coefficients tabulated for different classes of aircraft [4]. The horizontal tail volume coefficient (V_{HT}) for a general aviation twin engine aircraft was selected where $V_{HT} = 0.80$. With the horizontal tail moment arm (l_{HT}) determined by the fuselage size, the horizontal tail area (S_{HT}) was calculated using Equation 8 where c_{wing} is the chord and S_{wing} is the area of the main wing.

$$V_{HT} = \frac{l_{HT} \cdot S_{HT}}{c_{wing} \cdot S_{wing}} \quad (8)$$



4.3.5 Directional Stability

The main parameter for directional stability is the size and position of the vertical stabilizer. These parameters were determined through iterative calculations based on tail volume coefficients tabulated for different classes of aircraft [4]. The vertical tail volume coefficient for a general aviation twin engine aircraft was selected ($V_{VT} = 0.08$), and the vertical tail arm (l_{VT}) was assumed to be the same as the horizontal tail. The vertical tail area was calculated using Equation 9 where b_{wing} is the wingspan.

$$V_{VT} = \frac{l_{VT} \cdot S_{VT}}{b_{wing} \cdot S_{wing}} \quad (9)$$

4.3.6 Control Surface Sizing

The high MTOW played a significant role in control surface design and sizing. It was determined that flaps were necessary to achieve safer landing speeds. They were sized to 26.6% of the chord and span nearly half of the wing. Roll control is provided by ailerons sized to 26% of the chord with a 33.5 in.² control surface area for each aileron. The elevator was sized to 28% of the horizontal stabilizer chord and the rudder to 38.6% of the vertical stabilizer MAC.

4.4 Drag Performance

An aerodynamic drag analysis of the aircraft was performed starting from the wind tunnel experimental drag polar for the infinite aspect ratio wing. Finite wing induced drag was added resulting in the finite wing drag polar given by the equation below with the design aspect ratio and at the selected Reynolds number of 550,000.

$$C_D = C_{D,0} + \frac{C_L^2}{\pi \cdot AR \cdot e} \quad (10)$$

Coefficients of drag for the main aircraft components were calculated using the component drag build-up method shown in Equation 10 above, which estimates the flat plate skin friction then applies corrections for geometric differences and interference effects [3]. The sensor and towline drag coefficients were determined using plots and methods in Hoerner's *Fluid Dynamic Drag* where the sensor was approximated as a blunt cylindrical body in axial flow and the towline was approximated as a cylinder in cross flow with a correction applied for the angle of the towline [5]. All drag coefficients were normalized to the nominal aircraft wing area. The drag coefficients at the estimated high-speed cruise lift coefficient of 0.31 are listed in Table X with a breakdown by percentage contribution to total drag in the adjacent pie chart.



Table 14: Component Drag Normalized to Wing Area at $C_L = 0.31$.

| Component | C_D |
|------------------------------|--------|
| Wing ($C_{D,0} + induced$) | 0.0142 |
| Fuselage | 0.0086 |
| Horizontal Stabilizer | 0.0023 |
| Vertical Stabilizer | 0.0017 |
| Front Landing Gear | 0.0034 |
| Main Landing Gear | 0.0037 |
| Sensor | 0.0013 |
| Towline | 0.0052 |
| Mission | C_D |
| M1 & M2 | 0.0339 |
| M3 | 0.0403 |

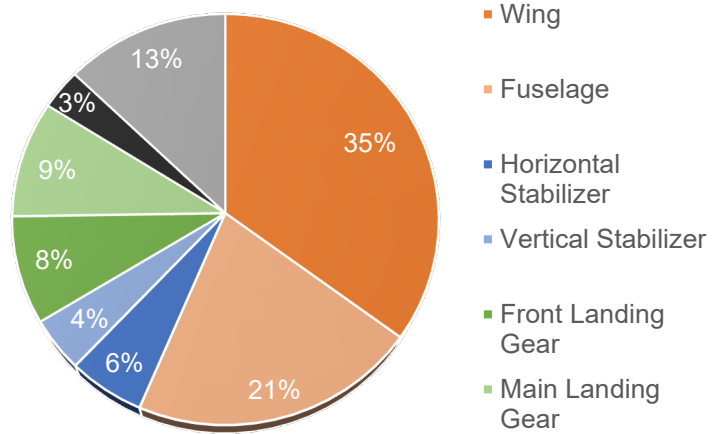


Figure 14: Component Drag Breakdown at $C_L = 0.31$.

Coefficients of drag for main components were then added to the finite wing drag polar to obtain the drag polar for the complete aircraft with and without the sensor deployed.

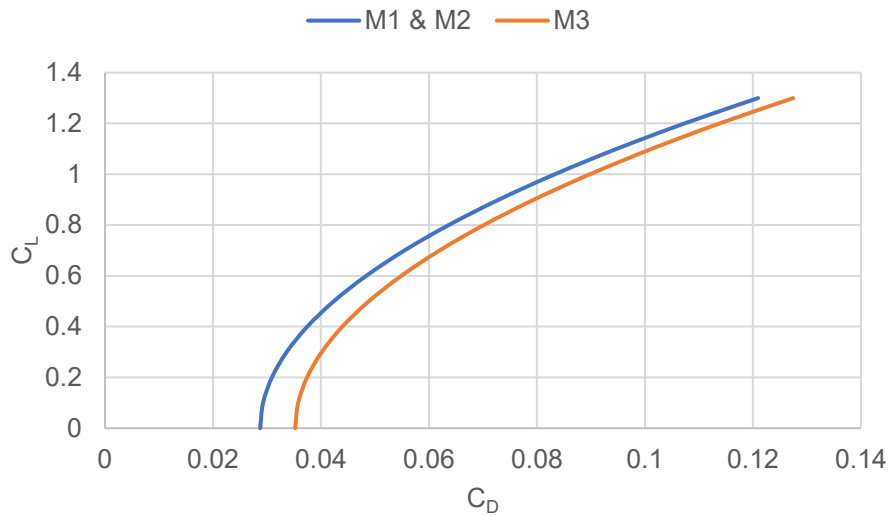


Figure 15: Drag Polar of Complete Aircraft for Each Mission.

4.5 Propulsion Design

4.5.1 Battery Selection

A LiPo battery was chosen to power the propulsion system due to its high energy density. Using Equation 11 for total available energy seen below, six cells in series were selected for the LiPo battery because they maximized the total energy in the aircraft while staying under the 100 Wh competition limit by 0.1 Wh. This selection offered a good balance between energy and capacity, as seen in Table 15 below.

$$Total\ Energy\ (Wh) = Nominal\ Voltage\ (V) \times Capacity\ (mAh) \quad (11)$$



Table 15: Total Stored Battery Energy Comparison.

| Battery Type | Nominal Voltage | Capacity | Total Energy |
|--------------|-----------------|----------|--------------|
| 6S | 22.2V | 4500mAh | 99.9Wh |
| 8S | 29.6V | 3250mAh | 96.2Wh |

4.5.2 Motor Selection

To determine the Kv rating needed for the aircraft's motors, a range of propellers large enough to provide adequate thrust while small enough to have safe ground clearance were considered. Equation 12 was used to find the thrust force as a function of RPM for each of these propellers. In this equation, cruise speed, V_o was given by the statistical analysis as 115 ft/s, and propeller dimensions are used to calculate the thrust F_{Thrust} produced.

$$F_{thrust} = (4.392399 \times 10^{-8}) \times RPM \frac{d^{3.5}}{\sqrt{pitch}} \times [(4.2333 \times 10^{-4})RPM \times pitch - V_o] \quad (12)$$

The above equation was put into MATLAB in order to show the RPM output needed by the motors to reach the required thrust values for missions two and three (based on expected mission drag). Figure 16 below was used to observe that the required thrust for each mission was reached at values ranging from 8,500 to 12,000 RPM.

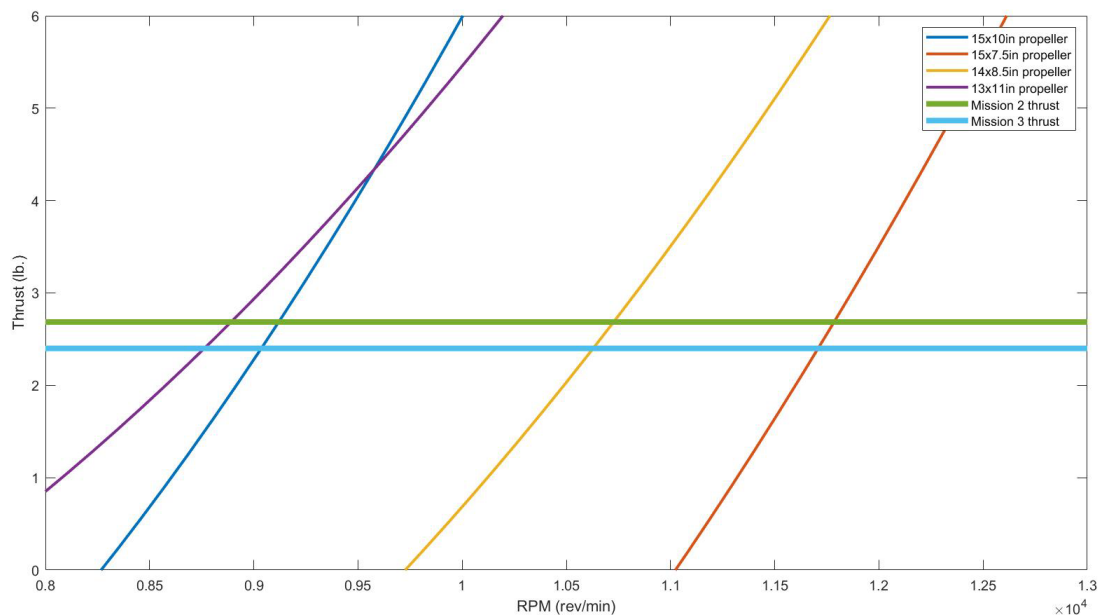


Figure 16: Thrust Output Versus Motor RPM using Equation 12.




Using Equation 13 below, assuming a battery at 95% charge (24.9V), a Kv rating from 341 to 482 $\frac{RPM}{Volt}$ would allow the motor to supply the propulsion system with adequate RPM to reach the required thrust for missions two and three.

$$Total\ Revolutions\ per\ Minute\ (RPM) = kV\ Rating \left(\frac{RPM}{Volt} \right) \times Battery\ Voltage\ (Volts) \quad (13)$$



Knowing the Kv range needed for competition motors, eCalc was used to compare the theoretical performance of motors. Three final motors were selected and compared using a figure of merit table, seen in Table 16 below. Kv ratings on the higher end of this range were used to provide greater thrust output for the propeller chosen.

Table 16: Motor Selection Figure of Merit Analysis.

|  | |  |  |  |
|---|-------------|---|--|---|
| Figures of Merit | Weighting | KDE4215XF-465 Kv | Turnigy SK3 5055-430 Kv | Rimfire .55-480 Kv |
| Max RPM | 0.25 | 5.00 | 4.00 | 5.00 |
| Cost | 0.25 | 2.00 | 5.00 | 3.00 |
| Weight | 0.20 | 5.00 | 3.00 | 4.00 |
| Frontal Area | 0.10 | 4.00 | 3.00 | 5.00 |
| Max Power | 0.20 | 3.00 | 5.00 | 2.00 |
| Total | 1.00 | 3.75 | 4.15 | 3.7 |

4.5.3 Propeller Selection

MATLAB was used to compare a wide range of prospective propellers. To achieve this required thrust, Equation 12 was used at full throttle (10,700 RPM from Equation 13). These parameters were put into MATLAB and the force produced by each propeller diameter that provides a safe ground clearance was plotted as a function of pitch, as seen in Figure 17.

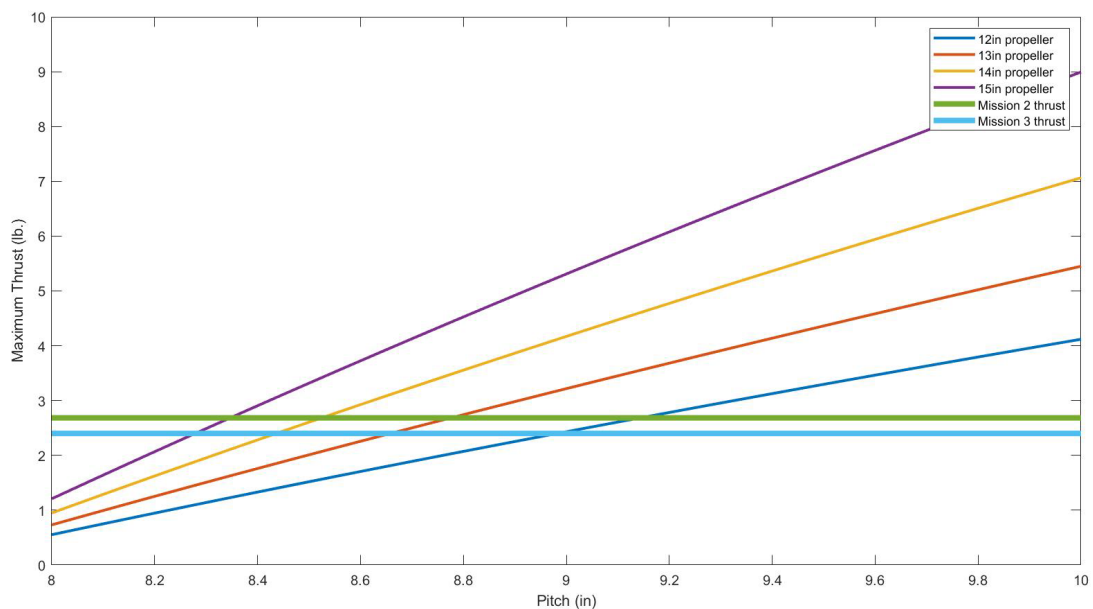


Figure 17: Maximum Thrust Produced for Each Propeller Diameter as A Function of Pitch.



The point at which a propeller line intersects a required mission thrust line represents a diameter and pitch combination that can surpass the drag force of the aircraft (and sensor during M_3). There is a wide range of propellers that can satisfy the required thrust for each mission. This data was validated with a thrust/current analysis, detailed in Section 8.3.2 to determine the propeller that would provide the most thrust without sacrificing flight time.

4.6 Payload Design

The deployment and retraction mechanism were built on a separate module for ease of modification and subsystem testing. The module includes a bomb bay door mechanism, a winch, and an alignment mechanism.

4.6.1 Bomb Bay Door Mechanism

Bomb bay doors were chosen as a point of exit and entry of the towed sensor. Two servo motors are used to individually actuate each door to achieve more throw. A tape hinge design was chosen for simplicity. To decide the rating of the servo motors needed, a calculation of static force by Bernoulli's principle was used. Assuming the aircraft is flying at a maximum speed of 124.1 ft./s and air density of 0.076 lb./ft³, the internal to external pressure difference on both doors was calculated to be 0.108 psi.

$$P_{in} - P_{out} = \frac{1}{2} \rho_{\infty} v^2 \quad (14)$$

With a total door area of 25 in.², the total static force on both doors was calculated to be 2.7 lb. The minimum torque needed from each servo motor was calculated to be 0.131 ft.-lb. with a 0.59 in. servo horn and a push rod connected 0.3 in. away from the door hinge. Figure 18 shows the bomb bay door servo configuration.



Figure 18: Bomb Bay Door Servo Configuration.

4.6.2 Winch Actuation

A 3D printed winch was selected as the deployment and retraction mechanism for the sensor because of its simplicity. A 0.75 in. drum was selected for the winch based on the space available for the winch assembly and the geometry needed to integrate bearings into the winch drum. A geared DC motor was selected to actuate the



winch with a speed of 400 RPM. With the geared DC motor, the retraction time was reduced to approximately 5.5 s. This speed was verified using retraction testing with a wind tunnel. This allows the sensor to be retracted quickly into the aircraft to reduce the flight time needed for M_3 before landing. Equation 14 was used to calculate the required motor RPM for a desired retraction time and drum size.

$$\frac{\text{Towline length (in)}}{\text{Drum Circumference (in)}} = \text{Required rev} \quad \frac{\text{Required rev}}{\text{Desired time (s)}} * \frac{60 \text{ (s)}}{\text{min.}} = \frac{\text{rev}}{\text{min.}} \quad (14)$$

4.6.3 Towline Material

Monofilament fishing line was used for the initial towlines for the sensor. However, it was difficult to integrate the communication wires for the sensor with the monofilament. Thin enamel wires were selected for the communication wires because of their small diameter to reduce the size and, consequently, the drag of the towline as much as possible. Strands of Kevlar thread were used to make it easier to combine the towline material and the communication wires. Different means of combining the wires with the thread were tested including a loose braid and twisting. The loose braid did not keep the strands tight enough together and the wires caught and broke during deployment and retraction. The tight twist worked much better to keep the strands together. A drill was used to tightly twist the Kevlar and enameled wire strands together.

4.6.4 Sensor Light Electronics

The electronics onboard the sensor was designed to allow activation of three sequenced LEDs with a single signal wire. Brightness and space efficiency were prioritized in the design. A small microcontroller, the Seeduino Xiao, was selected as the smallest off-the-shelf microcontroller board available. Constant current LED drivers instead of resistors to limit LED current allowed for the maximum efficiency and lowest heat production for the required brightness. Transistors allowed for actuation of each of the lights in a sequenced manner from the microcontroller when a digital signal was received over the tow line. The schematic of the sensor electronics is shown below in Figure 19.

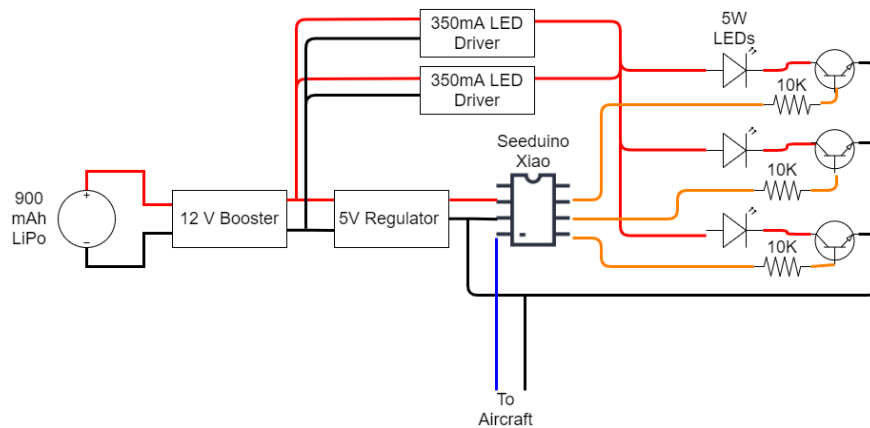


Figure 19: Sensor Electronics Schematic.



4.6.5 Sensor Fin Sizing

The sensor fins were sized to maximize the distance between the center of pressure (C_p) and the CG of the sensor. The C_p was estimated as the centroid of the projection of the sensor. A MATLAB simulation calculated the optimal length of the sensor fins to move the C_p as far as aft as possible. The graphic from this simulation is shown in Figure 19 with the red dotted line showing the most aft CG position and corresponding fin size. A fin length of approximately 3 in. was selected.

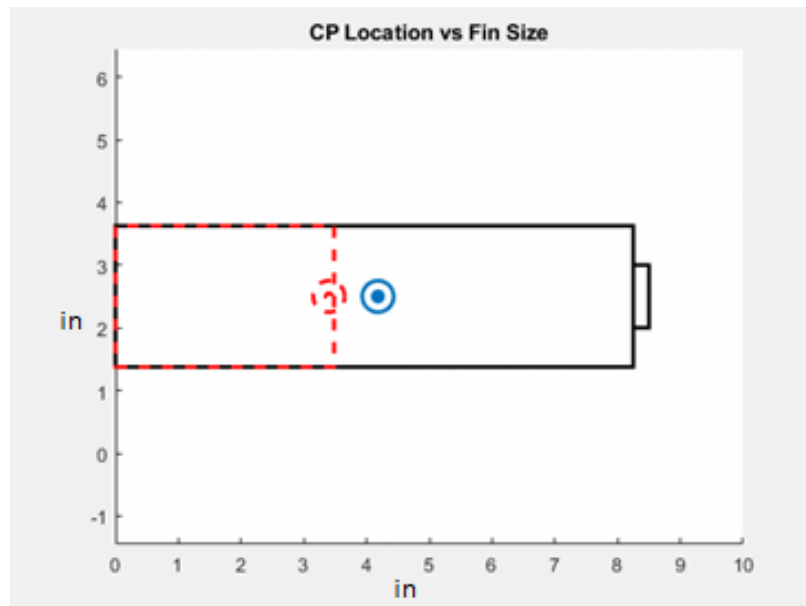


Figure 20: Simulation of C_p vs Fin Sizing.



5 Detail Design

5.1 Work Breakdown Structure

Castor Volant

1 Aerodynamics and Structures

1.1 Fuselage

1.1.1 Structure

1.1.2 Skin

1.2 Nose

1.2.1 Structure

1.2.2 Skin

1.3 Landing Gear

1.3.1 Front Structure

1.3.2 Aft Structure

1.3.3 Wheels

1.4 Main Wing

1.4.1 Ribs

1.4.2 Main Spar

1.4.3 Ailerons

1.4.4 Flaps

1.4.5 Spar Sleeve

1.4.6 Mylar Covering

1.4.7 Mounting Plate

1.4.8 Dowels

1.4.9 Aft Spar

1.4.10 Motor Nacelle

1.5 Empennage

1.5.1 Vertical Stabilizer

1.5.2 Rudder

1.5.3 Horizontal Stabilizer

1.5.4 Elevator

2 Propulsion and Controls

2.1 Propulsion System

2.1.1 Motors

2.1.2 Propellers

2.1.3 ESCs

2.1.4 Battery

2.2 Control System

2.2.1 Receiver

2.2.2 Servos

2.2.3 Control Horns

2.2.4 Pushrods

2.2.5 Transmitter

2.3 Telemetry

2.3.1 GPS

2.3.2 Voltage Monitor

2.3.3 Current Monitor

2.3.4 Barometric Altimeter

3 Payload and Manufacturing

3.1 Sensor Structure

3.1.1 Sensor Body

3.1.2 Nosecone

3.1.3 Fins

3.1.4 Ballast

3.1.5 Tow Point

3.2 Sensor Electronics

3.2.1 Battery

3.2.2 LEDs

3.2.3 PWM Parser

3.2.4 Electronics Mount

3.2.5 Misc. Electronics

3.3 Deployment Winch

3.3.1 Motor

3.3.2 Spool

3.3.3 Slip Ring

3.3.4 Winch Structure

3.3.5 Tow Cables

3.3.6 Doors

3.3.7 Sensor Module

3.3.8 Alignment Arm

3.3.9 Limit Switch

3.4 Shipping Container

3.4.1 Body

3.4.2 Lid

3.4.3 Storage Array

4 Aircraft Assembly

4.1 CAD Assembly

4.1.1 Prototype 1

4.1.2 Prototype 2

4.1.3 Prototype 3

4.1.4 Final Aircraft

4.2 Drawings

4.2.1 Three View Drawing

4.2.2 Structural Arrangement

4.2.3 Systems Configuration

4.2.4 Payload Configuration



5.2 Dimensional Parameters Table

Table 17: Final Design Dimensional Parameters and Specifications.

| Wing | | Propulsion | |
|-----------------------------------|-----------|----------------------------------|------------------|
| Airfoil | SG 6040 | Motor | Turngy SK3 5055 |
| Wingspan (in.) | 60.00 | Kv Rating | 430 |
| MAC (in.) | 8.65 | Motor Weight (oz.) | 13.33 |
| Planform Area (in. ²) | 519.00 | Power Rating (W) | 1750 |
| Aspect Ratio | 6.94 | No-Load Current (A) | 70 |
| Aileron % Chord | 26.00 | Internal Resistance (Ω) | 0.019 |
| Aileron Area (in. ²) | 33.48 | Controls | |
| Flap % Chord | 26.60 | Receiver | FrSky X8R |
| Flap Area (in. ²) | 24.45 | Main Wing Servo | HS-85MG |
| Incidence Angle | 0 | Empennage/LG Servo | LKY61 |
| Horizontal Stabilizer | | ESC | Aerostar 80A |
| Airfoil | NACA 0012 | Battery | Turnigy 4500mAh |
| Span (in.) | 19.22 | Battery Cell Count | 6 |
| Mean Chord (in.) | 5.91 | Battery Pack Voltage (V) | 25.4 |
| Planform Area (in. ²) | 113.00 | Battery Pack Weight (oz.) | 26.28 |
| Taper Ratio | 1.00 | Propellers | |
| Elevator % Chord | 28.00 | Mission 1 | 14 x 8.5 |
| Elevator Area (in. ²) | 32.29 | Mission 2 | 15 x 10 |
| Vertical Stabilizer | | Mission 3 | 15 x 10 |
| Airfoil | NACA 0012 | Payload | |
| Span (in.) | 10.13 | Sensor Length (in.) | 8.50 |
| Mean Chord (in.) | 7.29 | Sensor Diameter (in.) | 1.00 |
| Planform Area (in. ²) | 79.66 | Sensor Weight (oz.) | 7.05 |
| Taper Ratio | 0.50 | Shipping Container Count | 14.00 |
| Rudder % Chord | 35.80 | Retraction Motor | 25:1 6V DC Motor |
| Rudder Area (in. ²) | 23.74 | Tow Line Length (in.) | 85 |
| Fuselage | | Sensor Lumens (LM) | 500 |
| Total Length (in.) | 50.90 | Sensor Battery | 900mAh 18350 |
| Nose Cone Length (in.) | 10.15 | Landing Gear | |
| Tail Length (in.) | 22.75 | Height (in.) | 4.00 |
| Tail Sweep Angle | 12.45 | Width Span (in.) | 11.73 |
| Diameter (in.) | 7.00 | Length Span (in.) | 10.94 |

5.3 Structural Characteristics

5.3.1 Wing Structure

The wing is made up of balsa wood ribs and covered with a mylar skin. The primary structural member of the wing is a balsa dowel wrapped in three zero-degree carbon fiber plies. There is a second carbon dowel in the rear of the wing to help support and align the wing, while also providing additional torsional and bending strength. The spars themselves are mounted directly to the fuselage, with the left and the right sides of the wing sliding



onto the spar and being held in place by a bolt that threads into the plane. Balsa wood leading and trailing edges also provide structure for the mylar during the heat shrinking process, as well as some small structural loads. The spacing on the ribs at 2 in. was shown to be the best balance between mylar sag and weight saving.

5.3.1 Fuselage Structure

The fuselage is designed to have a large internal volume with minimal drag while being able to withstand the forces of flight shown in Figure 21. A simple nosecone is located in front, with the top half being removable to allow for easy insertion of the battery and internal maintenance of the plane. The structure itself is made up of a Kevlar epoxy mix with a network of internal stringers to provide the strength required to lift a heavy payload. The top of the structure has a nacelle that matches the shape of the wing for minimal drag, and it also serves as a mounting point. There are two holes in the nacelle that allow the spars to pass through, providing a distributed load along the mounting point to prevent damage to the structure during high G maneuvers. The internal volume is large enough to fit two sets of shipping container assemblies to carry as much cargo as possible without reducing flight capability.

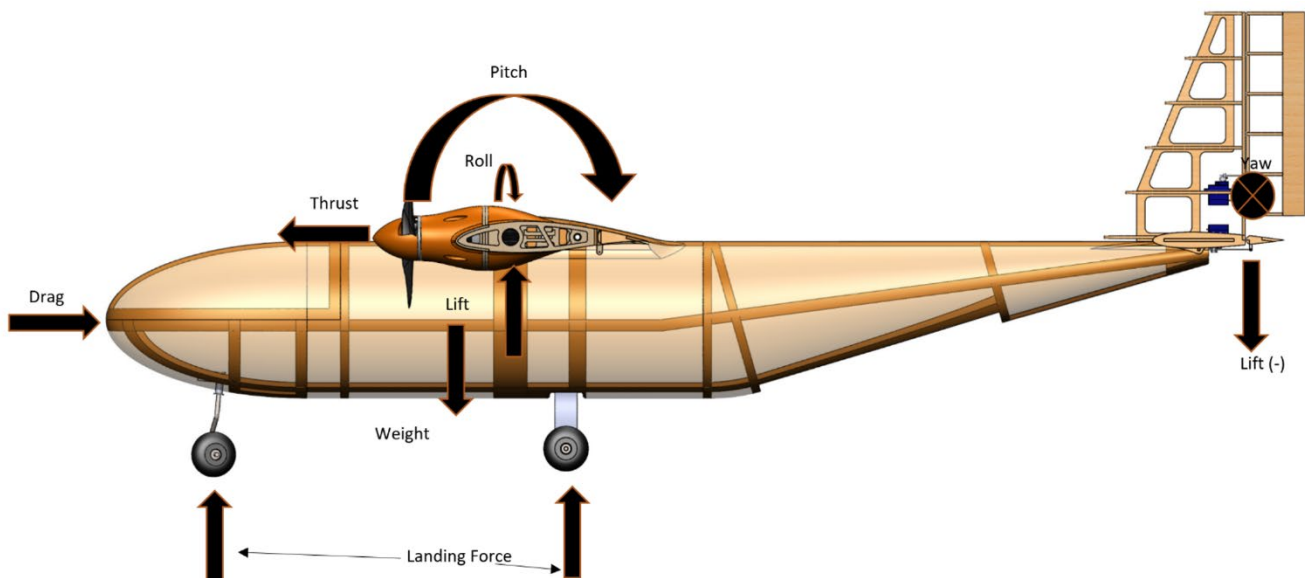


Figure 21: Loading Paths on Fuselage.

5.4 System Selection and Integration

5.4.1 Wing Integration

Due to the high wing loading of the aircraft, it was decided that mounting the front and rear spars of the wing directly to the fuselage would be the strongest way to fasten the wing to the aircraft. Each spar will be adhered to holes in the fairing portion of the fuselage with an epoxy resin. The rest of the wing will be preassembled and then slid on to the spars and attached to the fuselage with nylon fasteners as shown in Figure 22 below.

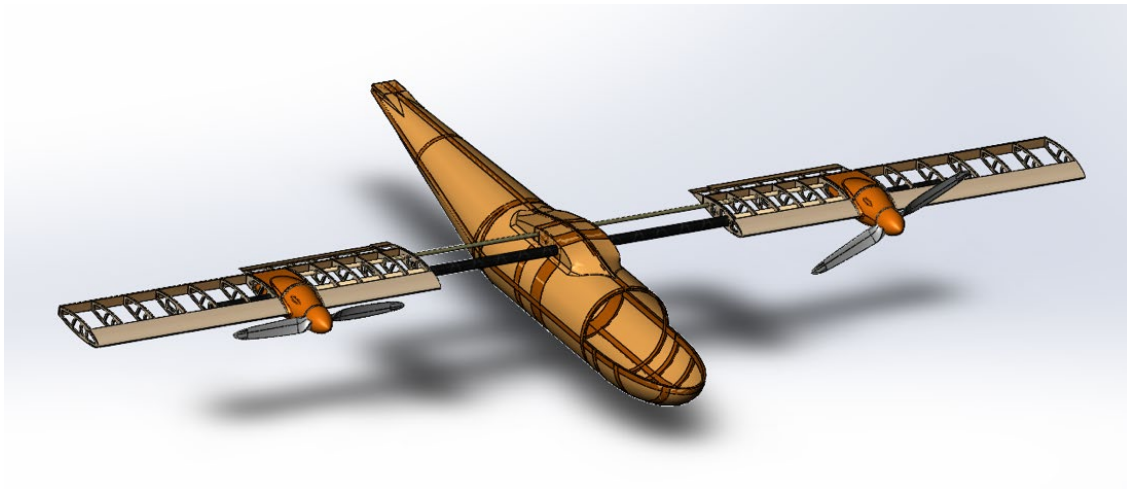


Figure 22: Wing Integration with Fuselage.

5.4.2 Empennage Integration

The horizontal and vertical stabilizers feature a plywood mounting plate along which balsa ribs are glued. The two mounting plates run the entire span to transfer the aerodynamic loads and feature lightening holes. The vertical mounting plate protrudes through a slot in the horizontal mounting plate to align the two components which are glued together. Additional structure comes from trailing edge balsa stringers. Four nylon bolts attach the horizontal stabilizer mounting plate to the fuselage which is reinforced with balsa at the mounting location.

5.4.3 Control Surface Integration

The aircraft has four types of control surfaces all made with balsa-monokote construction: ailerons, flaps, rudder, and elevator. The ailerons, rudder, and elevator are attached to the main lifting surfaces with nylon RC aircraft hinges. Slots on the trailing edge of the main lifting surfaces and the leading edge of the control surfaces align the two components. The nylon hinges are inserted through the slots and glued in place. Because the flap only has deflection in one direction, tape hinges are used to affix the flap to the wing and create a continuous surface for reduced drag.

5.4.4 Sensor Deployment and Recovery Mechanism

The deployment and recovery for the sensor is accomplished using a small winch actuated with a geared DC motor. The winch support, drum, and motor support are all 3D printed from PLA material. For the physical communication connection between the aircraft and sensor, a slinging is used to integrate the wires from the towline through the winch drum. The slinging allows the wires to remain stationary while the drum rotates around the slinging. For quick deployment of the sensor, the drum of the winch freewheels to deploy the sensor. A bearing is added opposite the DC motor to reduce friction as much as possible. A one-way bearing is added to the motor shaft to allow the winch to freewheel for deployment and for the DC motor to retract the sensor back into the aircraft. To turn the motor off once the sensor is retracted, a limit switch was included. This allows the sensor to press against the switch and shut off the motor once fully retracted. A section view of the motor and



winch is shown in Figure 24 below. Visible in this view is the one-way bearing on the motor shaft, the bearing opposite the motor, the space between the bearings for the slipping, and the DC motor.

The towline for the sensor is constructed of Kevlar thread and mag wire. Three strands of Kevlar thread are needed for strength and two strands of mag wire for control of the sensor electronics. For symmetry, four strands of Kevlar were used for the towline. Two strands of Kevlar and one mag wire were tightly twisted together, and this was repeated with the remaining strands. The tight twist kept the individual strands from catching or tangling during deployment and retrieval of the sensor.

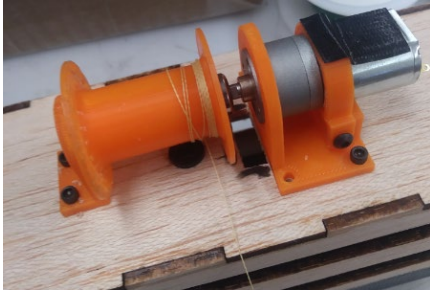


Figure 23: Deployment and Retraction Winch.

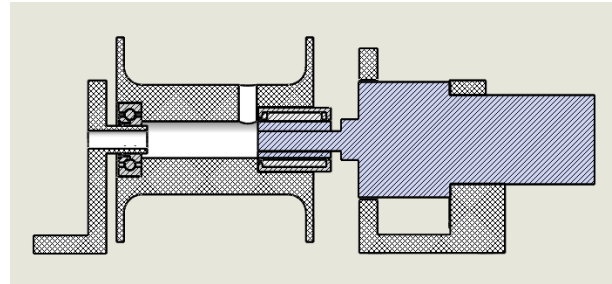


Figure 24: Section View of Winch Mechanism.

5.4.5 Module and Sensor Integration

The winch is integrated into a balsa module that also houses the bomb bay doors and alignment arm. The module is used to make it easier to insert and remove the sensor retraction apparatus between the different missions. The module consists of a winch mechanism, bomb bay doors, and an alignment arm attached to the module structure. The sensor is attached to the towline and reeled into the module. The module is fitted into the fuselage and secured with bolts. Figure 25 shows the sensor module with the winch, alignment arm, bomb bay doors, and sensor. Note that the near side of the module has been removed to show the internal configurations.

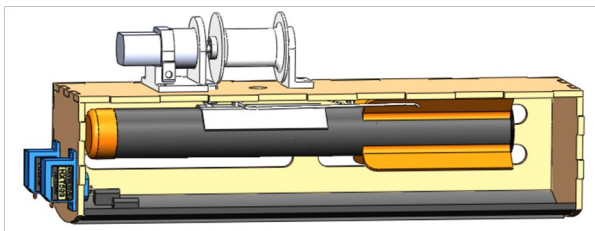


Figure 25: Sensor Module System.

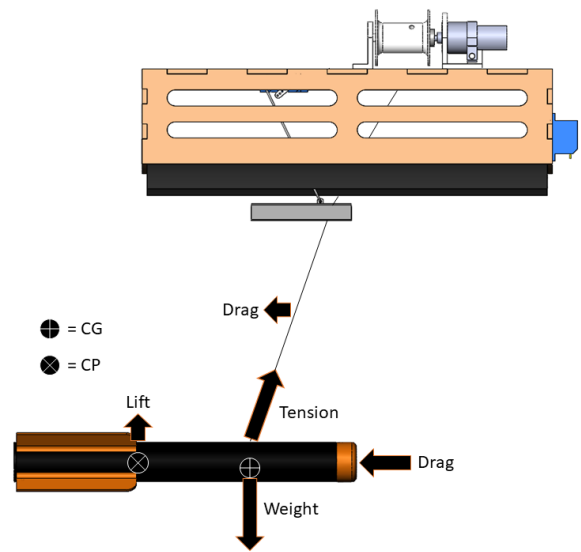


Figure 26: Loading Path on Sensor When Deployed.



5.4.6 Shipping Container and Shipping Container Simulator Integration

Four balsa wood spacers are used to hold one shipping container and thirteen shipping container simulators in the fuselage. Each spacer has seven circular holes in a honeycomb configuration shown in Figure 27. Seven shipping containers are fitted into two spacers and two groups of shipping containers are slid into the fuselage from the front. The sensor arrays are shown inside the fuselage in Figure 28 below.

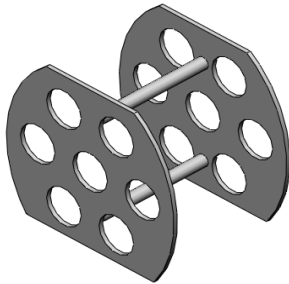


Figure 27: Shipping Container Spacer.

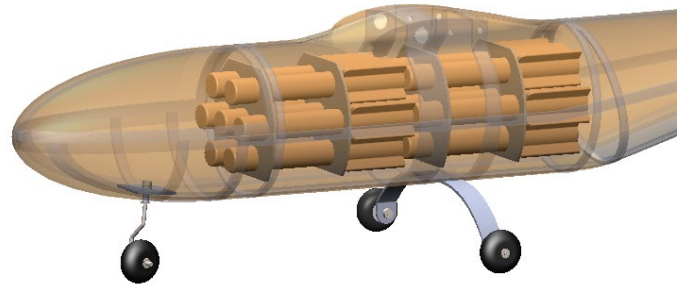


Figure 28: Shipping Container Arrays in Fuselage.

5.4.7 Landing Gear Integration

The main landing gear is placed about 2 in. aft of the CG so that the elevator can rotate the aircraft on takeoff. It is attached to the fuselage by inserting it through a slot in the fuselage and glued in using fiberglass reinforcements that transfer the load to the fuselage, which is additionally braced with a balsa bulkhead to distribute the loads and reduce stress concentrations. The fiberglass construction gives the landing gear high specific stiffness, allowing it to be lightweight while maintaining sufficient stiffness to prevent the aircraft from striking the ground. The front landing gear was positioned to carry 15% of the aircraft weight. This provides enough load for effective steering but prevents the nose wheel from wobbling. The wheelbase between the front and main landing gear is roughly 13.5 in. The front landing gear is steerable with a servo mounted a few inches aft in the fuselage and is secured to the fuselage with four 0.25 in. bolts.

5.4.8 Propulsion Integration

The motor on each wing is protected by a 3D-printed nacelle cover, which decreases form drag and are removable to decrease integration and maintenance times. Each ESC is located inside the wing with an opening design to reduce operating temperature as wind from the wing passes over them, decreasing their chance of overheating. The battery is located on the latitudinal center of the fuselage floor and moved in order to place the mission CG on the wing spar, since the battery is the heaviest internal component. The receiver is in the front of the fuselage with the two antennae secured on the outside in orthogonal directions to each other to ensure a stable connection with the transmitter during flight.

To avoid human error and decrease the time of integration and maintenance, all wires were color-coded to the corresponding receiver channel as seen in Figure 29. Labels were added to the aircraft transmitter according to



the controls and switches shown in Figure 30 below to reduce pilot error during flight and operation of the payload systems. Wire management was continually optimized in order to reduce weight from unnecessary wires and to lower the chance of failure due to faulty or unstable wired connections. All connections were covered using heat shrink to further decrease the chance disconnection during flight.

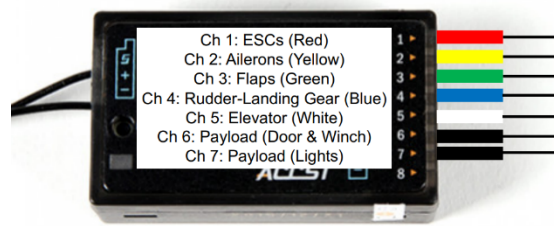


Figure 29: Color-Coded Receiver Channels.



Figure 30: Transmitter Switch and Control Layout.


To maximize the speed of ground missions, the organization of the electrical components, and provide a consistent location of the CG, an organization tray will be implemented in the nose of fuselage. This tray will provide a consistent and sturdy location for the receiver and battery and allow for logical routing for all the wires branching from the receiver out to the control surface servos and ESCs.

5.5 Weight and Balance

Tracking the aircraft CG is essential for determining static longitudinal stability to ensure safe and controlled flight. The weight and position of each component relative to the datum 12 in. in front of the nose was measured and tabulated in Table 18. During initial flight testing, various CG locations were tested to determine an ideal location to reduce trim at the target cruise speed. It was determined positioning the CG at the quarter chord was optimal to reduce trim and thus drag. The battery position is adjusted slightly for each mission to ensure the CG remains in the same location. The first section shows the components in mission one. The following two sections represent missions two and three. Components such as the motors and propellers are assumed to be evenly positioned about the longitudinal axis such that no moment is created.



Table 18: Weight and Balance for All Flight Missions.

|  | | Mission 1: Empty Weight | | |
|---|---------------------------|-------------------------|--------------------------|-----------------------------|
| | | Weight | Longitudinal CG Location | Longitudinal Moment Created |
| WBS | Component | [lb.] | [in.] | [lb.*in.] |
| 1.10 | Fuselage | 0.85 | -35.55 | -30.32 |
| 1.30 | Forward LG | 0.27 | -18.62 | -5.03 |
| 1.40 | Main LG | 0.22 | -33.89 | -7.46 |
| 1.50 | Main Wing Structure | 1.55 | -32.33 | -50.11 |
| 1.6.1 | Vertical Stabilizer | 0.14 | -63.21 | -9.04 |
| 1.6.3 | Horizontal Stabilizer | 0.25 | -62.83 | -15.71 |
| 2.1.1 | Motors | 1.66 | -29.11 | -48.32 |
| 2.1.2 | Propellers | 0.16 | -27.22 | -4.46 |
| 2.1.3 | ESCs | 0.36 | -33.60 | -12.16 |
| 2.1.4 | Battery | 1.64 | -18.90 | -31.00 |
| 2.2.1 | Receiver | 0.04 | -18.90 | -0.76 |
| 3.00 | Sensor Module | 0.57 | -46.21 | -26.48 |
| Total | | 7.72 | -31.18 | -240.84 |
| Mission 2: Shipping Container Flight | | | | |
| 2.1.4 | Battery | 1.64 | -18.90 | -31.00 |
| 3.40 | Shipping Container Module | 7.23 | -31.27 | -226.08 |
| Total | | 14.95 | -31.22 | -466.92 |
| Mission 3: Sensor Flight | | | | |
| 2.1.4 | Battery (1) | 1.64 | -18.90 | -31.00 |
| 2.1.4 | Battery (2) | 1.64 | -27.40 | -44.94 |
| 3.10 | Sensor | 0.44 | -45.27 | -19.92 |
| Total | | 9.80 | -31.18 | -305.69 |

5.6 Flight Performance Parameters

Expected performance for the three flight missions is shown in Table 19 below. These values are based on flight test data and on the competition specified parameters for the missions to calculate an expected mission score.

Table 19: Flight Mission Performance Parameters.

| Performance Parameter | Mission I | Mission II | Mission III |
|----------------------------|-----------|------------|-------------|
| Number of Laps | 3 | 3 | 22 |
| Mission Time (min) | 2.5 | 1.5 | 10 |
| Mission Speed (mph) | 70 | 78 | 80 |
| Lap Time (sec) | 45 | 39 | 38 |
| Sensor Number | - | 14 | 1 |
| Payload Weight (oz) | - | 98.8 | 7.1 |
| Average Voltage Drop (V) | 1.4 | 1.3 | 1.2 |
| Weight of Aircraft (lb.) | 9.9 | 17.6 | 12.1 |
| Mission Score | 1 | 2 | 3 |
| Total Mission Score | 6 | | |

5.7 Drawing Package

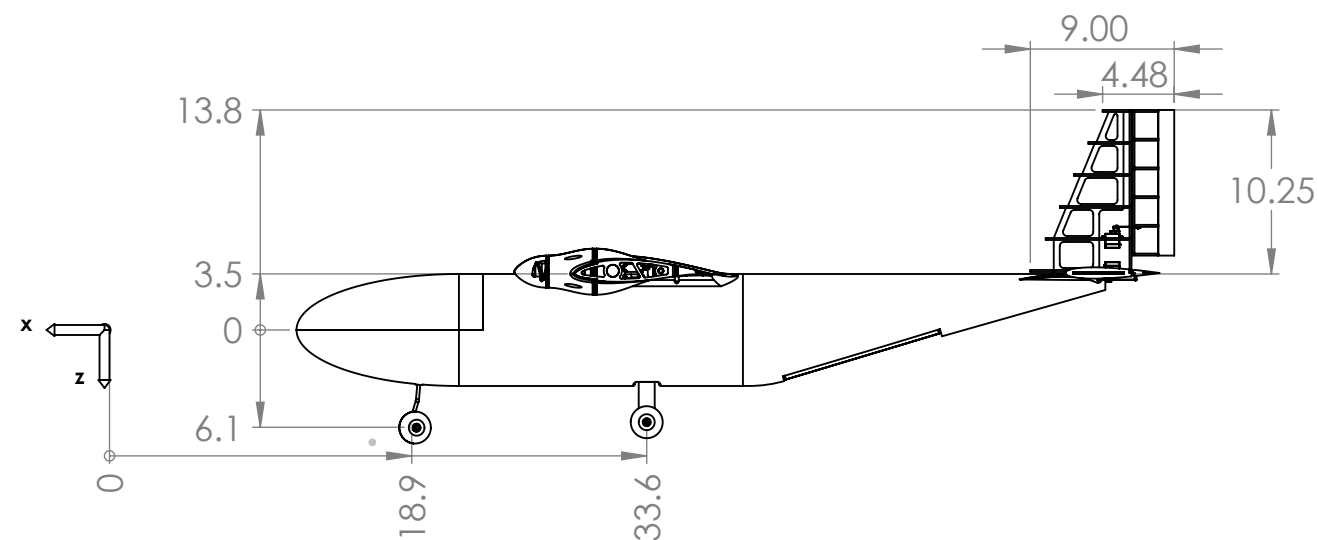
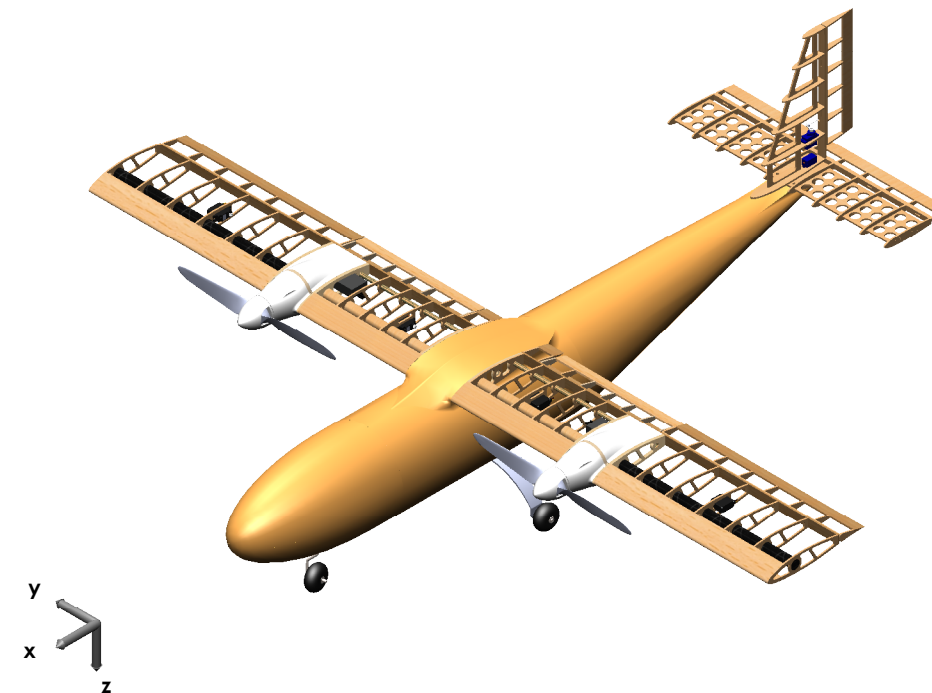
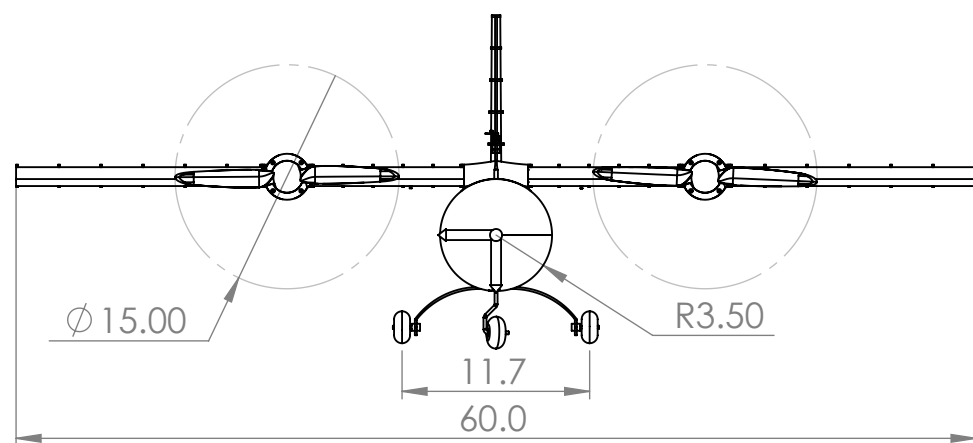
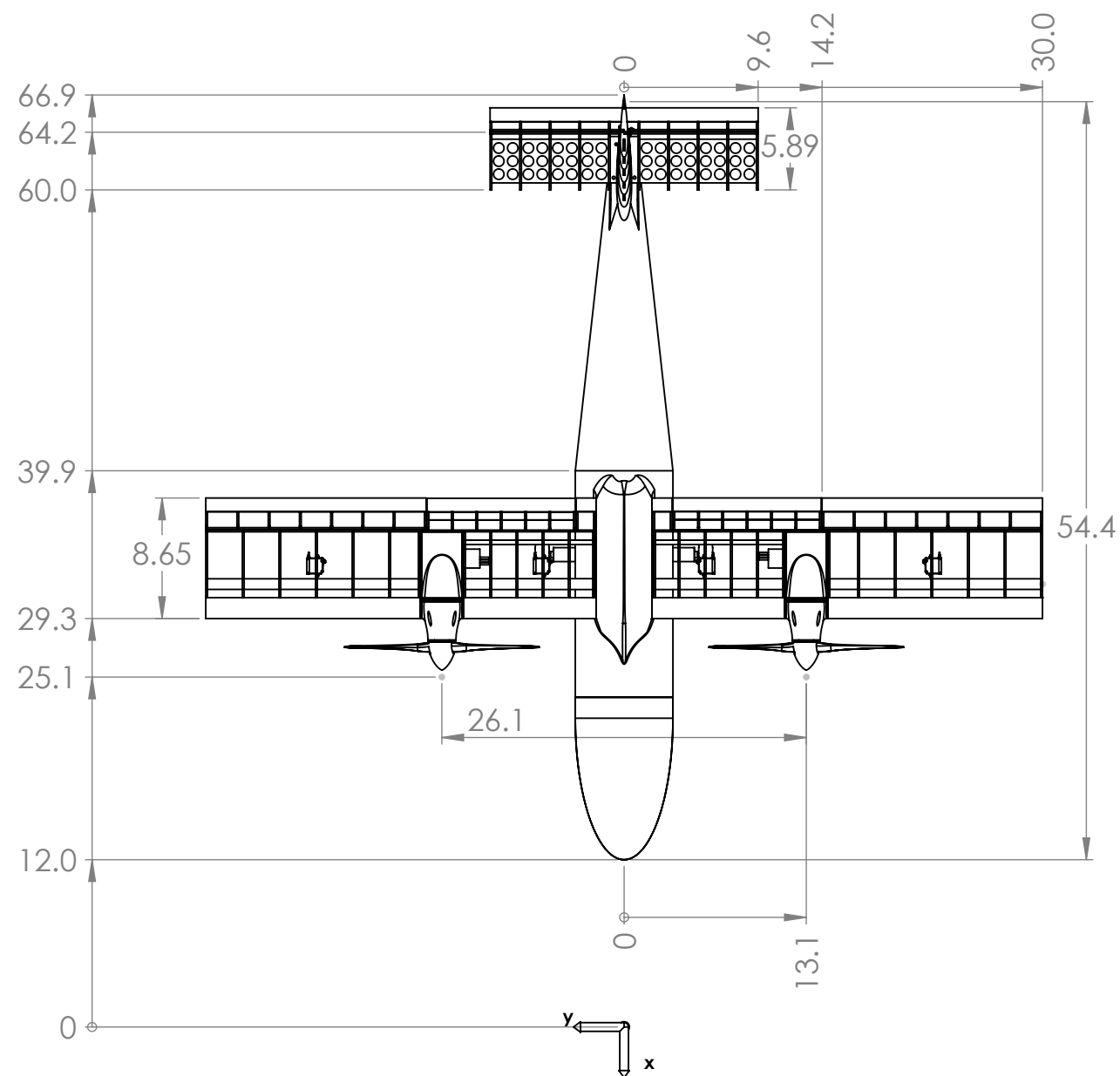
The following drawing package of the *Castor Volant* aircraft which includes a 3-View dimensional drawing, structural arrangements, subassembly system layout, and payload drawings.

4

3

2

1



ALL DIMENSIONS ARE
IN INCHES:

LINEAR DIMS:
.X \pm .1
.XX \pm .01

ANGULAR DIMS:
X $^\circ$ \pm 1 $^\circ$
X.X $^\circ$ \pm .1 $^\circ$

DRAWN:
JOSH BAMBERGER

CHECKED:
BRYAN KELLY

APPROVED:
GEORGE LE

DATE:
2/13/2021

TITLE:
AIRCRAFT THREE VIEW

| | | |
|------------------|--------------------|-----------------|
| SIZE B | DWG. NO. 4.2.01 | REV A |
| SCALE: 1:12 | | SHEET 1 OF 5 |

3

2

1

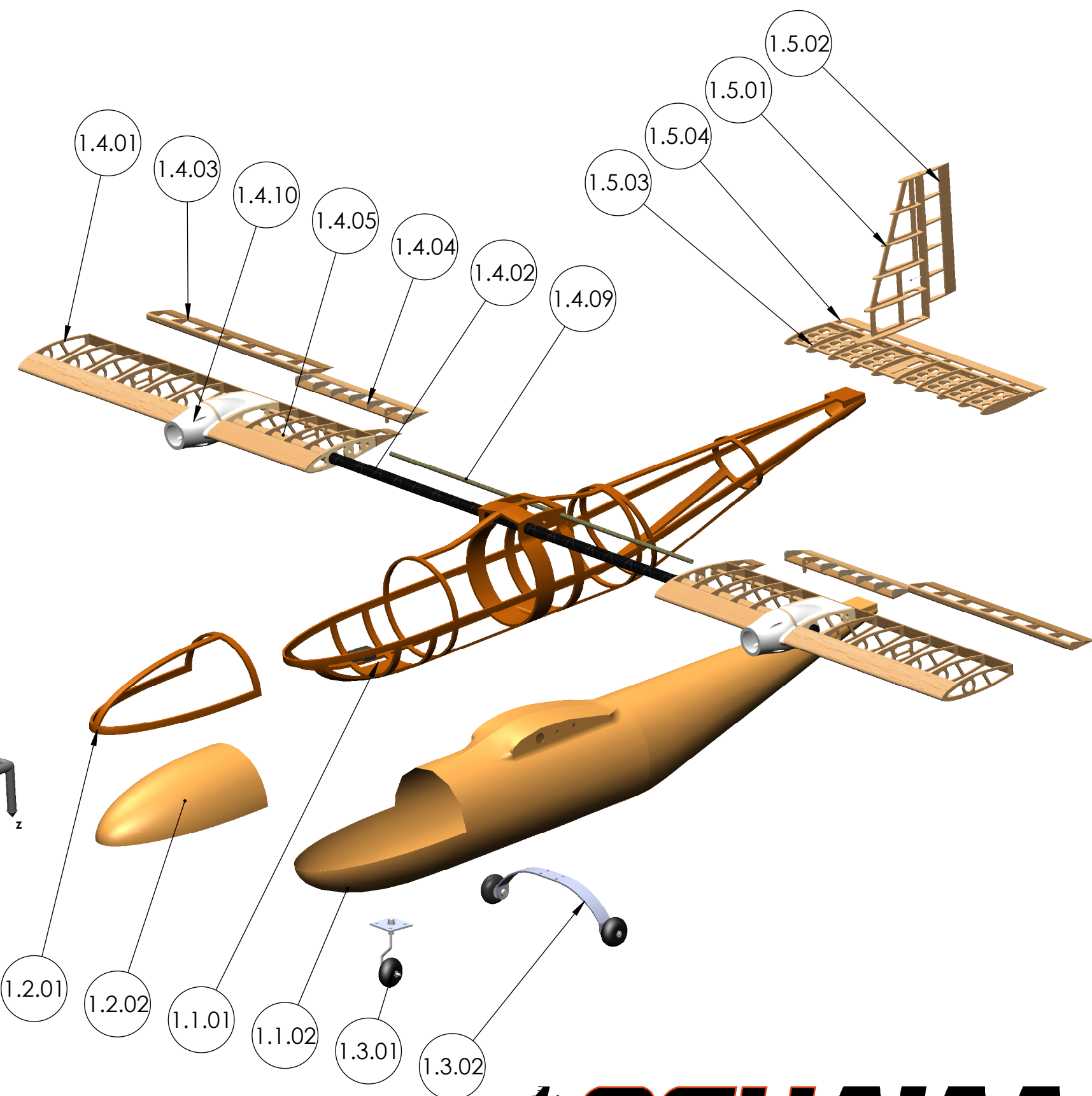
4

3

2

1

| WBS # | TITLE | DESCRIPTION/MATERIAL | QTY. |
|--------|------------------------------------|----------------------|------|
| 1.1.01 | LAYED UP FUSELAGE STIFFENER STRIPS | BALSA | 1 |
| 1.1.02 | FUSELAGE SKIN | KEVLAR/ARAMID | 1 |
| 1.2.01 | LAYED UP NOSECONE STIFFENER STRIPS | BALSA | 1 |
| 1.2.02 | NOSECONE SKIN | KEVLAR/ARAMID | 1 |
| 1.3.01 | FRONT LANDING GEAR | STEEL | 1 |
| 1.3.02 | AFT LANDING GEAR | FIBERGLASS | 1 |
| 1.4.01 | WING RIB | LASER CUT BALSA | 28 |
| 1.4.02 | MAIN SPAR | CARBON-EPOXY/BALSA | 1 |
| 1.4.03 | AILERON | BALSA/MYLAR | 2 |
| 1.4.04 | FLAPS | BALSA/MYLAR | 2 |
| 1.4.05 | SPAR SLEEVE | PAPER TUBE | 2 |
| 1.4.09 | AFT SPAR | CARBON-EPOXY TUBE | 1 |
| 1.4.10 | MOTOR NACELLE | PLA | 2 |
| 1.5.01 | VERTICAL STABILIZER | BALSA/MYLAR | 1 |
| 1.5.02 | RUDDER | BALSA/MYLAR | 1 |
| 1.5.03 | HORIZONTAL STABILIZER | BALSA/MYLAR | 1 |
| 1.5.04 | ELEVATOR | BALSA/MYLAR | 1 |



ALL DIMENSIONS ARE
IN INCHES:

LINEAR DIMS:
.X ± .1
.XX ± .01

ANGULAR DIMS:
X° ± 1°
X.X° ± .1°

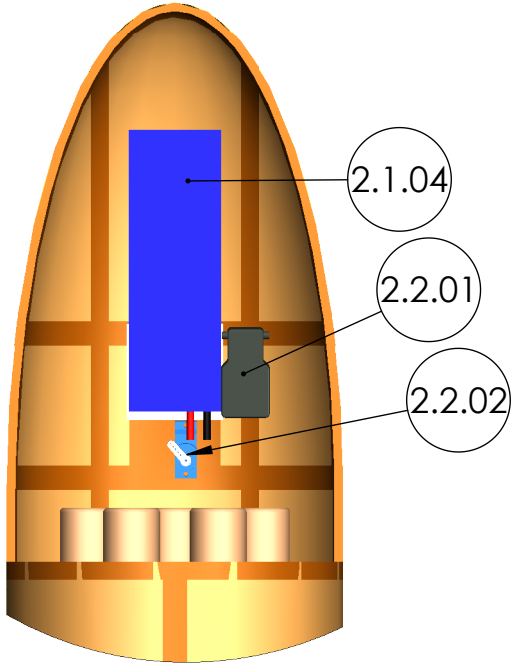
| | | | | |
|--------------------------|--|----------------------------------|--------------------|--------------|
| DRAWN: JOSH BAMBERGER | | TITLE: STRUCTURAL ARRANGEMENT | | |
| CHECKED: BRYAN KELLY | | | | |
| APPROVED: GEORGE LE | | SIZE B | DWG. NO. 4.2.02 | REV A |
| DATE: 2/13/2021 | | SCALE: 1:8 | | SHEET 2 OF 5 |

3

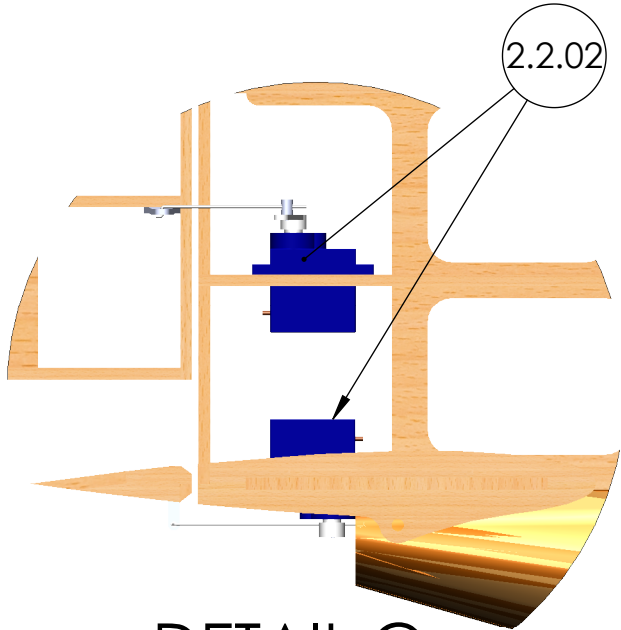
2

1

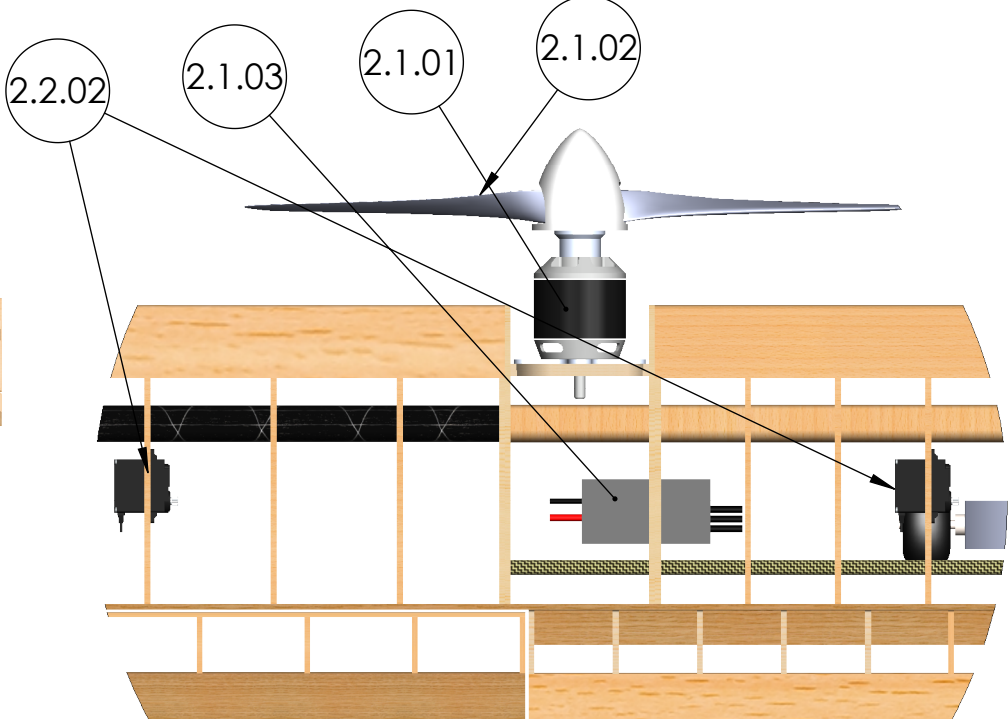
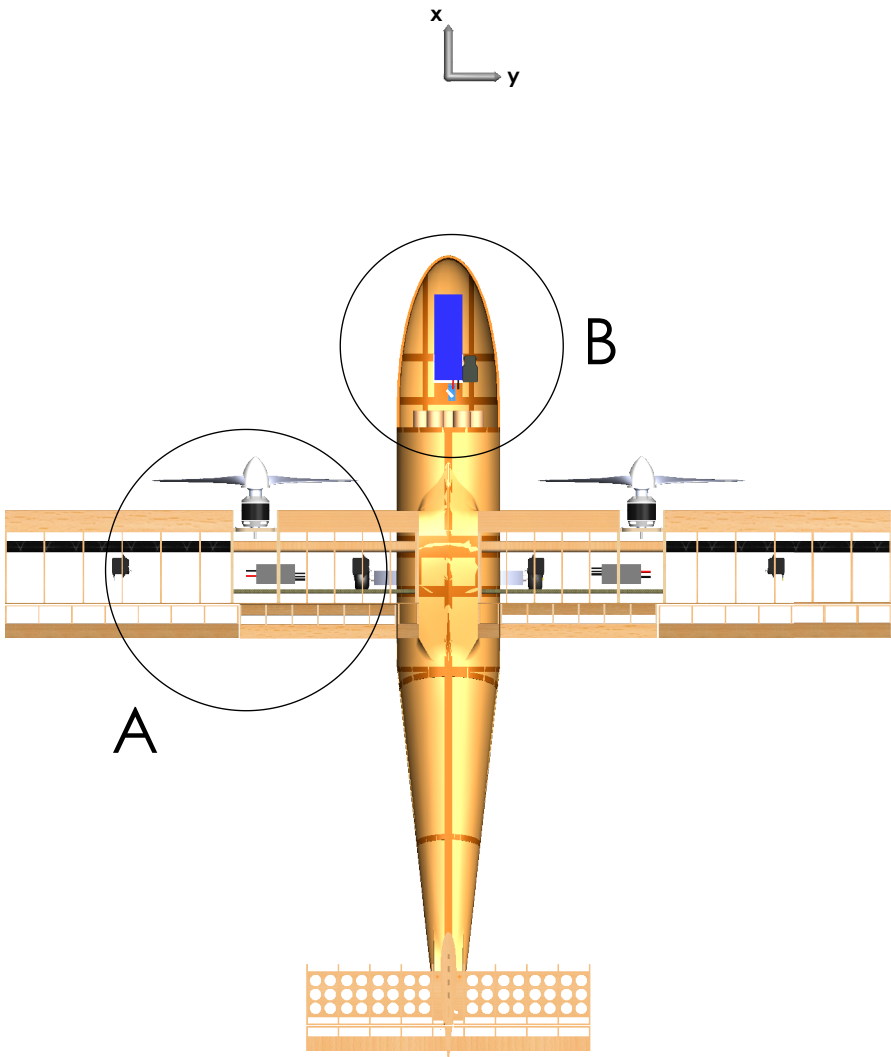
| WBS # | TITLE | DESCRIPTION | QTY. |
|--------|-----------------|---------------|------|
| 2.1.01 | SENSOR BODY | FIBERGLASS | 2 |
| 2.1.02 | SENSOR NOSECONE | BALSA | 2 |
| 2.1.03 | SENSOR FINS | KEVLAR/ARAMID | 2 |
| 2.1.04 | BATTERY | BALSA | 1 |
| 2.2.01 | LED | KEVLAR/ARAMID | 1 |
| 2.2.02 | MICROCONTROLLER | STEEL | 7 |



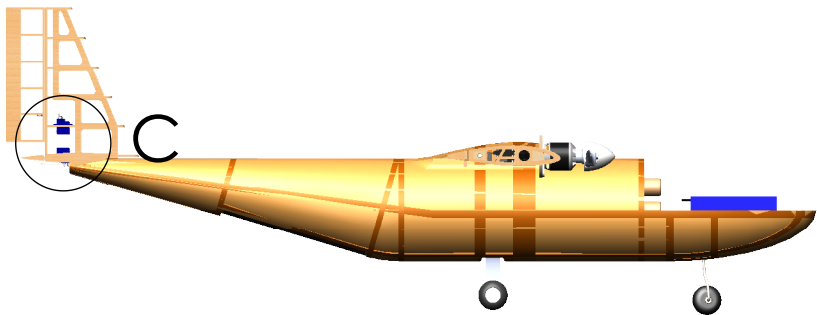
DETAIL B
SCALE 1 : 4



DETAIL C
SCALE 1 : 2



DETAIL A
SCALE 1 : 4



ALL DIMENSIONS ARE
IN INCHES:

LINEAR DIMS:
.X ± .1
.XX ± .01

ANGULAR DIMS:
X° ± 1°
X.X° ± .1°

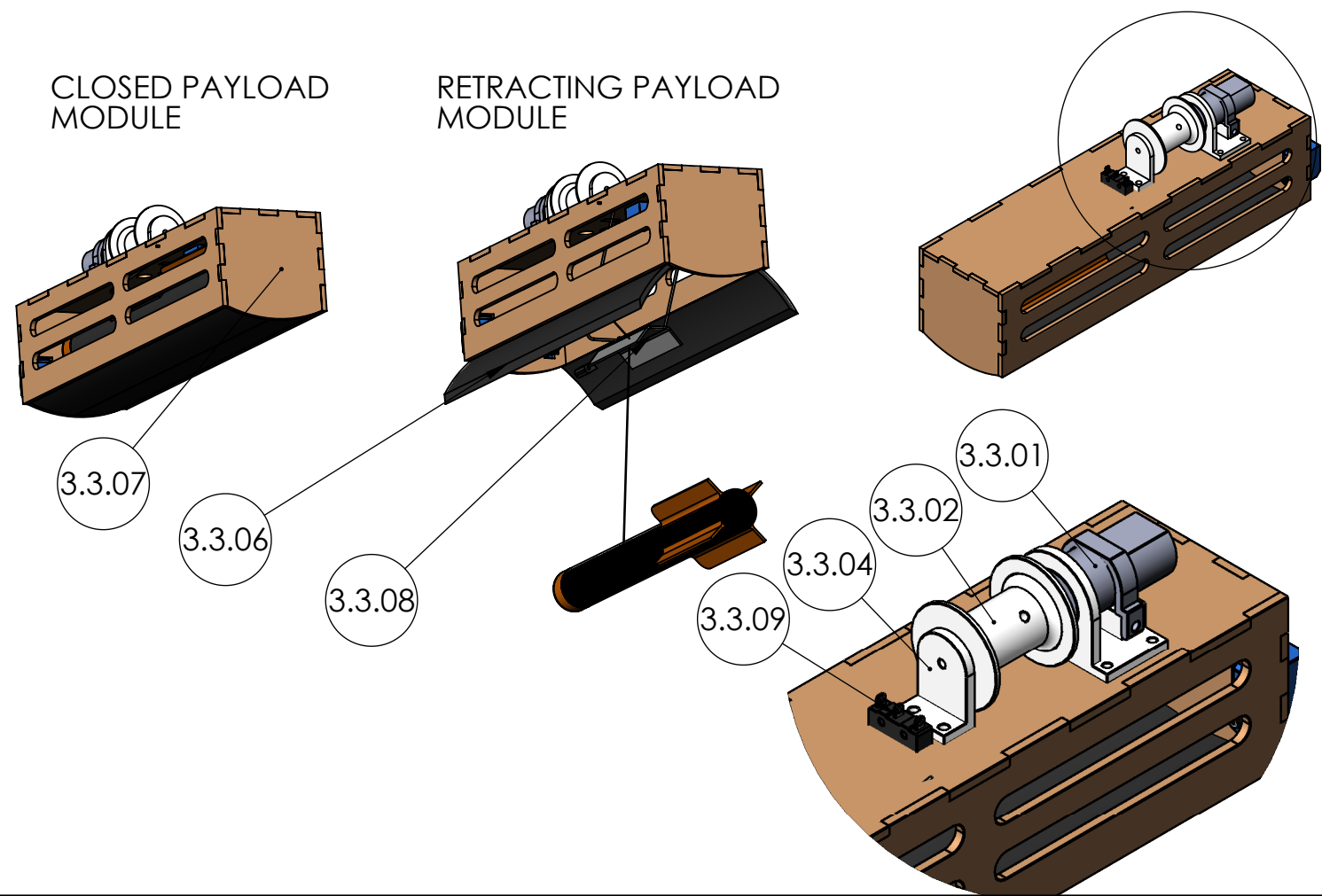
| | | | | |
|--------------------------|--|---|---------------------------|-----------------|
| DRAWN: JOSH BAMBERGER | | TITLE: PROPULSION/CONTROLS LAYOUT | | |
| CHECKED: BRYAN KELLY | | | | |
| APPROVED: GEORGE LE | | | | |
| DATE: 2/13/2021 | | SIZE B | DWG. NO. 4.2.03 | REV A |
| | | SCALE: 1:13 | | SHEET 3 OF 5 |

4

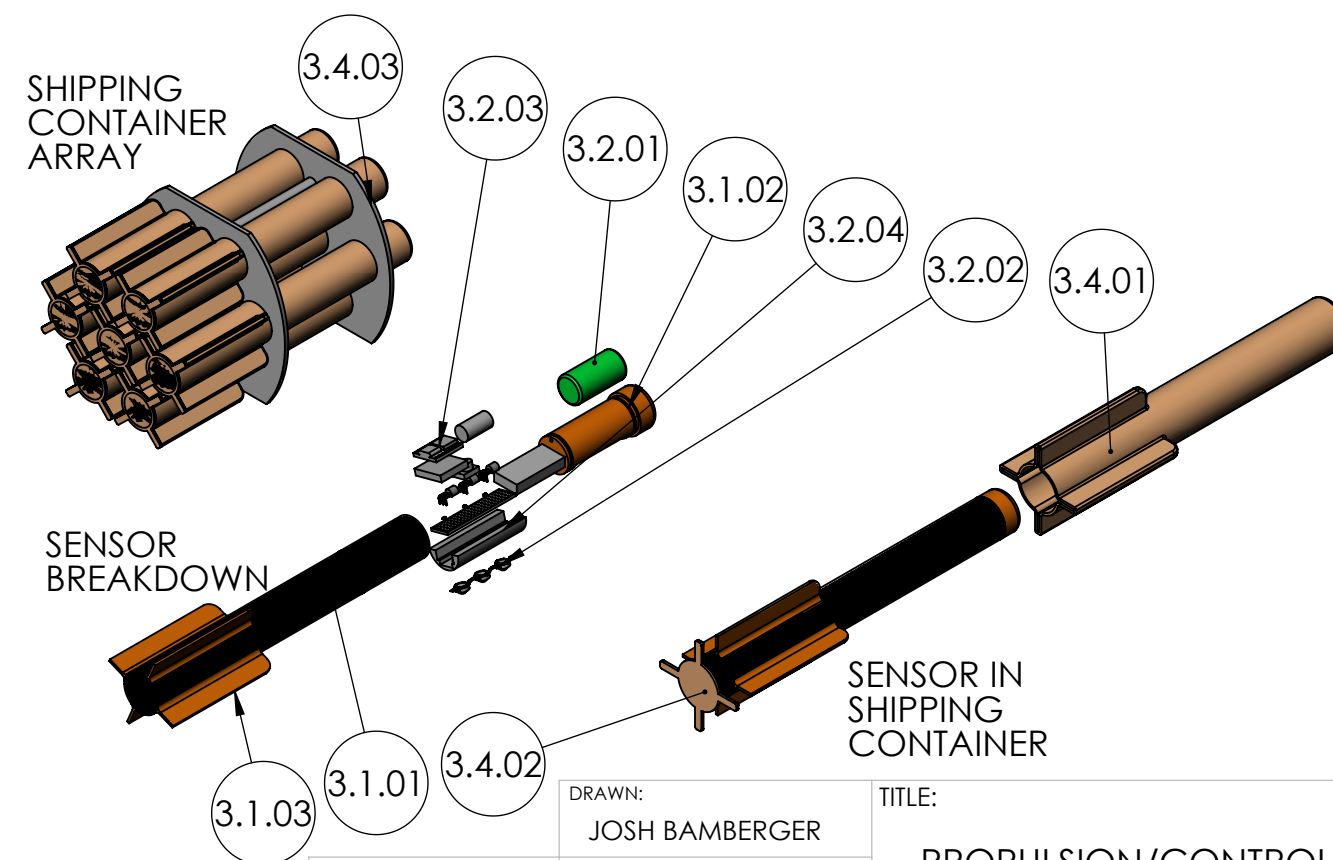
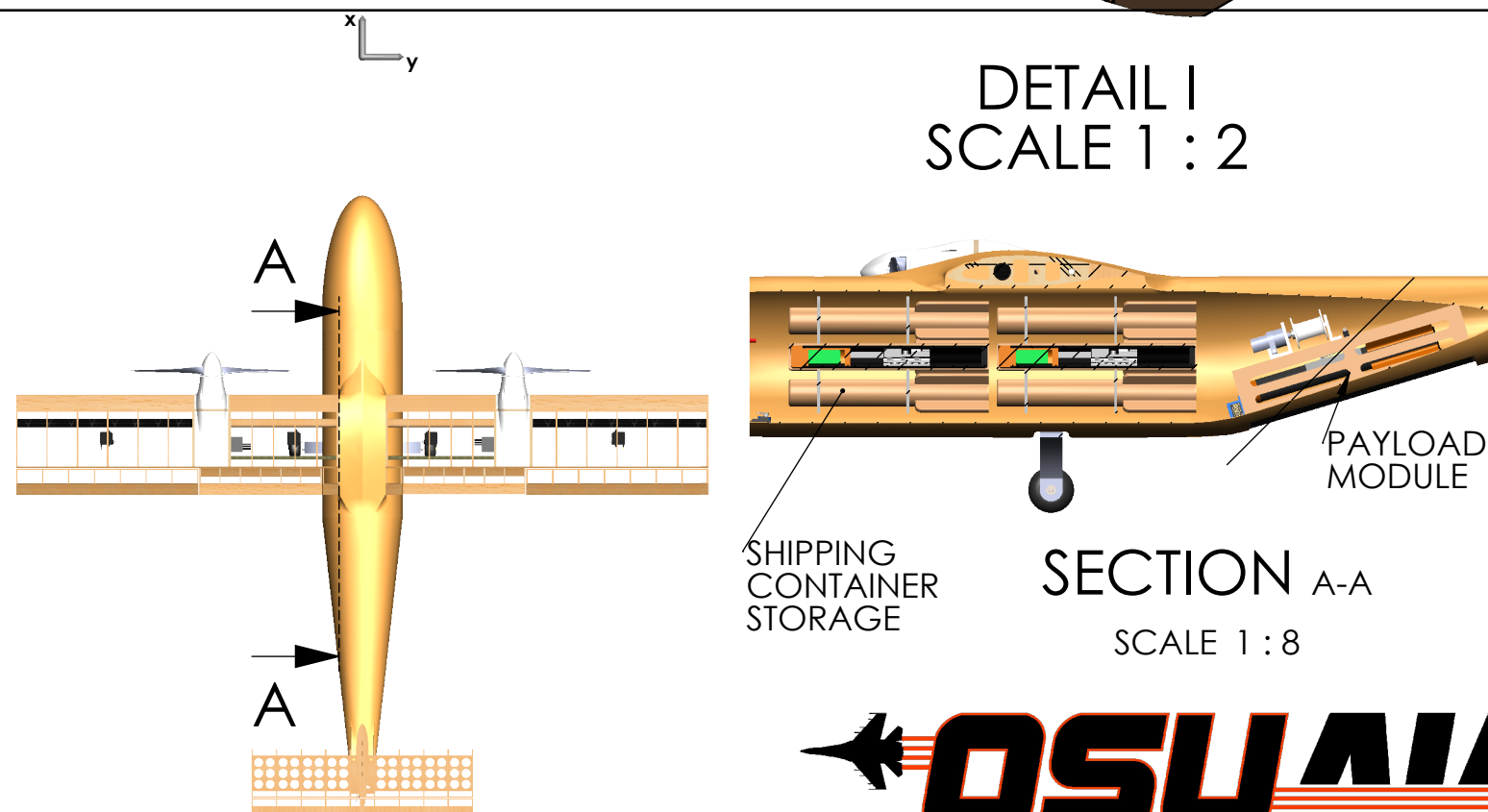
3

2

1

CLOSED PAYLOAD
MODULERETRACTING PAYLOAD
MODULE

| ITEM NO. | PART NUMBER | DESCRIPTION | QTY. |
|----------|------------------|----------------------|------|
| 3.1.01 | SENSOR BODY | ALUMINUM | 1 |
| 3.1.02 | SENSOR NOSECONE | PLA | 1 |
| 3.1.03 | SENSOR FINS | PLA | 4 |
| 3.2.01 | BATTERY | 900mAh 18350 BATTERY | 1 |
| 3.2.02 | LED | 5W LED | 3 |
| 3.2.03 | MICROCONTROLLER | SEEDUINO XIAO | 1 |
| 3.2.04 | ELEC. MOUNT | PLA | 1 |
| 3.3.01 | DC MOTOR | 6V 20:1 GEARMOTOR | 1 |
| 3.3.02 | WINCH SPOOL | PLA | 1 |
| 3.3.04 | WINCH STRUCTURE | PLA | 1 |
| 3.3.06 | PAYLOAD DOORS | PLA | 2 |
| 3.3.07 | PAYLOAD MODULE | BALSA | 1 |
| 3.3.08 | ALIGNMENT ARM | ALUM./BALSA | 1 |
| 3.3.09 | LIMIT SWITCH | N.O. MICRO SWITCH | 1 |
| 3.4.01 | SHIP. CONT. BODY | FIBERGLASS | 1 |
| 3.4.02 | SHIP. CONT. CAP | PLA | 1 |
| 3.4.03 | STORAGE ARRAY | BALSA | 1 |

DETAIL I
SCALE 1 : 2ALL DIMENSIONS ARE
IN INCHES:LINEAR DIMS:
X ± .1
.XX ± .01ANGULAR DIMS:
X° ± 1°
X.X° ± .1°DRAWN:
JOSH BAMBERGERCHECKED:
BRYAN KELLYAPPROVED:
GEORGE LEDATE:
2/16/2021TITLE:
PROPULSION/CONTROLS
LAYOUT

| | | |
|------------------|---------------------------|-----------------|
| SIZE B | DWG. NO. 4.2.04 | REV A |
| SCALE: 1:20 | | SHEET 4 OF 5 |

3

2

1



6 Manufacturing Plan

6.1 Manufacturing Materials

Foam was mostly utilized for rapid prototyping the fuselage to verify the aircraft configuration as seen in Figure 31 below. The foam was shaped using a hot wire along with saws and sandpaper. While foam is lightweight and has high manufacturability, it has higher density than balsa and has significantly lower specific stiffness than fiber-reinforced polymer (FRP) materials.



Figure 31: Prototype Aircraft Made from Foam.

Balsa was used in the construction of the wing and empennage ribs as a lightweight method to provide shape to the wing. Plywood was used over balsa in regions where additional strength was necessary. Balsa was additionally used as the sandwich core material in sections of the fuselage because of its shear strength, low density, and workability.

An aramid-epoxy composite was chosen for the fuselage due to its high specific strength and stiffness and its impact resistance. The use of FRP composites allows for a semi-monocoque fuselage that maximizes internal storage volume for specified maximum external envelope. Unidirectional carbon-epoxy prepreg tape applied around a balsa dowel provides stiffness and strength to the main spar of the wing. A wet layup fiberglass is used for reinforcing the sensor and manufacturing the shipping containers and was favored over prepreg materials for ease of manufacture and out of oven curing.

Steel, although heavier than the other materials used, was chosen for the primary material for the front landing gear for its high stiffness to carry the weight of the fully loaded aircraft.

3D printed plastic was used in the sensor deployment system and fins. Although it has low durability and is heavier than other plastics, it was chosen for its' ease of manufacturing.



6.2 Manufacturing Processes

The two materials comprising a majority of the aircraft components are FRP and balsa wood. A laser cutter was used to manufacture the balsa components for its high accuracy and repeatability. Some refinement was required using Dremel tools and sandpaper for integration. Aramid–epoxy prepreg was selected versus wet lay-up for its optimum fiber-to-resin ratio maximizing specific stiffness and strength. Components were manufactured at the OSU Composites Manufacturing Lab with vacuum bagging for consolidation and high temperature curing.

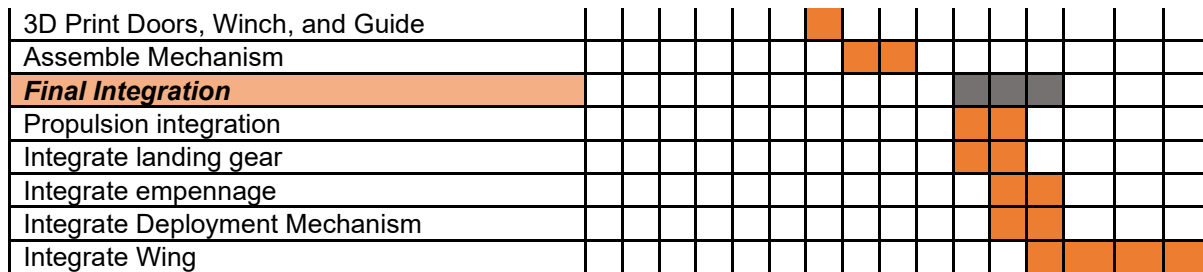
The shipping containers were largely composed of fiberglass-epoxy wet lay-up. The sensor body was manufactured from an aluminum tube with 3D printed fins. The 3D printed fins were adhered to the aluminum tube using epoxy. The nose cone was 3D printed to include a battery compartment and to fit tightly into the tubular body of the sensor.

6.3 Manufacturing Milestones

A schedule was created to support manufacturing management for the competition aircraft. Table 20 below depicts the schedule used for the aircraft with timeframes similar to those used for the prototypes.

Table 20: Manufacturing Milestones Schedule.

| OSU DBF 2020-21 | Feb | | | | March | | | | | | | April | | | |
|---------------------------------------|-----|--|--|--|-------|--|--|--|--|--|--|-------|--|--|--|
| Competition Aircraft Build | | | | | | | | | | | | | | | |
| Wings | | | | | | | | | | | | | | | |
| Laser Cut Balsa ribs | | | | | | | | | | | | | | | |
| Layup Carbon Fiber Spar | | | | | | | | | | | | | | | |
| Assemble and Mylar | | | | | | | | | | | | | | | |
| Empennage | | | | | | | | | | | | | | | |
| Laser cut balsa parts | | | | | | | | | | | | | | | |
| Assemble and Mylar | | | | | | | | | | | | | | | |
| Fuselage | | | | | | | | | | | | | | | |
| Fabricate MDF mold | | | | | | | | | | | | | | | |
| Layup Kevlar | | | | | | | | | | | | | | | |
| Cut Fuselage Bay Door | | | | | | | | | | | | | | | |
| Drill Wiring and Mounting Holes | | | | | | | | | | | | | | | |
| Paint | | | | | | | | | | | | | | | |
| Nosecone | | | | | | | | | | | | | | | |
| 3D Print | | | | | | | | | | | | | | | |
| Sensor and Shipping Containers | | | | | | | | | | | | | | | |
| Fabricate mold | | | | | | | | | | | | | | | |
| Fiberglass Wet Layup | | | | | | | | | | | | | | | |
| 3D Print Sensor Components | | | | | | | | | | | | | | | |
| Cut Steel Sensor Body | | | | | | | | | | | | | | | |
| Electronics Integration | | | | | | | | | | | | | | | |
| Assemble Sensor | | | | | | | | | | | | | | | |
| Landing Gear | | | | | | | | | | | | | | | |
| Cut and Bend Metal Struts | | | | | | | | | | | | | | | |
| Assemble landing gear | | | | | | | | | | | | | | | |
| Deployment Mechanism | | | | | | | | | | | | | | | |
| Laser Cut Balsa Parts | | | | | | | | | | | | | | | |



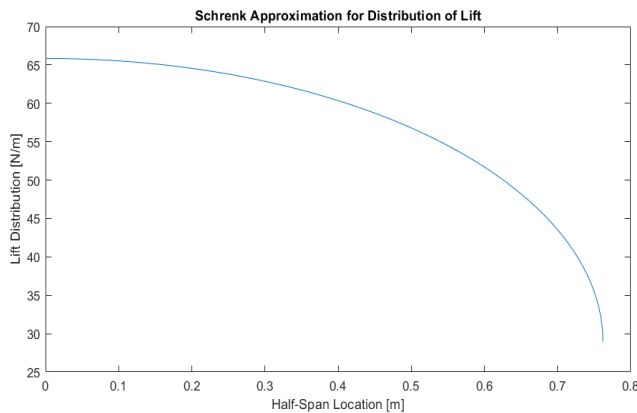


Figure 32: Half-Span Lift Distribution.

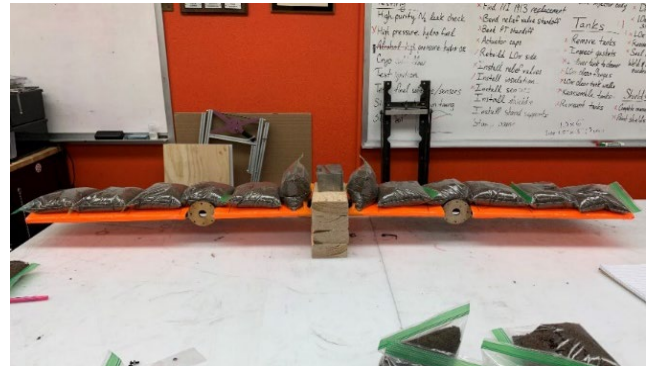


Figure 33: Wing Loading Testing Setup.

For this test, the wing was inverted, and its' center is secured in a G-loading fixture to prevent rotation during loading as shown in Figure 33 above. The appropriately weighted sandbags were placed along the wing working from the inner most stations out toward the wing tips. The deflection of the wing is measured prior to each increase in loading. The wing will be loaded up to a load factor of five in increments of one.

Table 22: Distribution of Load on Wing During Testing.

| | Station 1 (lb.) | Station 2 (lb.) | Station 3 (lb.) | Station 4 (lb.) | Station 5 (lb.) | Station 6 (lb.) |
|-------|-----------------|-----------------|-----------------|-----------------|-----------------|-----------------|
| n = 1 | 1.87 | 1.85 | 1.78 | 1.68 | 1.52 | 1.22 |
| n = 2 | 3.75 | 3.69 | 3.56 | 3.36 | 3.04 | 2.44 |
| n = 3 | 5.62 | 5.54 | 5.35 | 5.04 | 4.56 | 3.66 |
| n = 4 | 7.50 | 7.38 | 7.13 | 6.72 | 6.08 | 4.89 |
| n = 5 | 9.37 | 9.23 | 8.91 | 8.40 | 7.59 | 6.11 |

Wing Tip Testing: Wing tip was used to verify the aircraft's CG prior to flight. This test also satisfies the competition requirement that the team knows and marks the location of the CG on the exterior of the aircraft. The aircraft, in both loaded and unloaded configurations, is held up by each wing tip at different locations along the chord. The CG location is found when the aircraft longitudinal axis is horizontal.

7.1.2 Payload Testing

Drop Testing: Drop tests were carried out to validate the strength of the shipping containers and if the sensor was protected during the drop test portion of the ground mission. The sensor and shipping containers were dropped on all six sides starting at 10 in., the competition drop test height, and increased by increments of 10 in. until a final drop height of 30 in. was successfully completed, giving the shipping containers a safety factor of three based on drop height.

Wind Tunnel Testing: Wind tunnel testing allows for observation of the sensor behavior during deployment, flight, and retraction. A mockup of the aircraft fuselage is used to mimic flight orientation and the sensor will be hung by the payload module at the outlet of the wind tunnel to simulate airspeeds during flight. Testing validated



the aerodynamic stability of the sensor with selected blunt nosecone geometry. Testing is also performed to the reliability of the retraction and deployment of the sensor.



Figure 34: Deployment and Retraction Testing at Wind Tunnel.

7.1.3 Propulsion Testing

Static Testing: Static testing was used to validate prospective propulsion packages from initial eCalc simulations. Different motors, propellers, and ESCs could be easily compared for thrust output, torque, efficiency, and battery draw over time using an RC Benchmark thrust stand. This setup was placed into a reinforced metal cage to ensure the safety during operation as seen in Figure 35 to the right.



Propeller Optimization: Propellers with varying diameter and pitch found using the MATLAB thrust analysis were compared to find the dimensions that could provide the most thrust/current used, which would increase flight time and reduce the effects of voltage sag on thrust output. Each propeller was run on a six-cell LiPo battery at starting at exactly 24.9 V, while current and thrust values were recorded as throttle was slowly increased in increments of 1.5 lb. until the motor was stopped by the safety cutoff set at 10 lb.

Figure 35: Competition Motor on Thrust Stand.

7.2 Pre-Flight Checklists

Pre-flight checklists were made to ensure the repeatability of flight tests and to decrease the chance of failure during flight. This list is organized into four parts, the first being sub-team specific checklists and the last consisting of a final check on the runway to ensure the aircraft is operating as expected prior to takeoff and the safety of all bystanders. The checklist seen in Table 23 below was used to ensure each flight's data can be safely and accurately recorded.



Table 23: Pre-Flight Checklist.

| Aerodynamics and Structures | |
|------------------------------------|--|
| | Inspect all surfaces for cracks, weakness, and finish issues |
| | Inspect wing for damage to mylar wrapping |
| | Landing gear attached securely |
| | Wing and empennage attached securely |
| | Nose cone attached securely |
| | Verify aircrafts center of gravity is ideal for current flight |
| | Neutral control surfaces (or set to pilot preference) |
| Payload | |
| | Inspect sensor nose and fin for looseness and damage |
| | Secure sensor attachment points |
| | Ensure winch is secure and functioning correctly |
| | Check sensor electronics for functionality |
| | Ensure storage containers are preset and ready |
| | Check container/simulator installment and security |
| Propulsion | |
| | Ensure receiver antennae are secured in two orthogonal directions |
| | Battery is charged and appropriate for current flight mission |
| | Verify voltage of main battery pack (24.9V) |
| | Verify voltage of transmitter battery pack (6V) |
| | Correct fuse installed into propulsion system |
| | Battery and ESC's correctly secured in fuselage for CG |
| | Ensure motor is attached securely |
| | Check all wiring connections |
| | Receiver turned on, bound to transmitter |
| | Reprogram ESC with propellers not installed |
| | Kill-plug functioning as expected with propellers not installed |
| | Throttle cut functioning properly with propellers not installed |
| | Ensure all control surfaces are functioning correctly |
| | Ensure all control surfaces trimmed to neutral (or pilot preference) |
| | Ensure propeller is balanced and correct for current flight mission |
| | Test motor rotation direction (CLEAR PROP LINE and mount aircraft at a safe distance) |
| | Conduct range test with propellers not installed |
| | Install propeller and tighten securely |
| | Propeller in correct orientation for rotation (leading edge facing towards the fuselage) |
| On Runway | |
| | ALL PERSONS CLEAR OF PROP LINE |
| | ALL PERSONS CLEAR OF FLIGHT LINE |
| | Fire extinguisher on hand |
| | Test throttle, confirm correct propeller rotation direction |
| | Ensure aircraft tracks straight |
| | Check for evidence of motor vibration or frequency issues |

7.3 Flight Testing Plan

Flight tests are planned to evaluate the flight qualities and performance of each aircraft prototype. An on-board Eagle Tree telemetry system will be used to measure flight speed, position, current draw, voltage draw, pitch, roll,



and yaw angles. Aircraft mass and the longitudinal location of the CG will be measured and certified prior to each flight. Flight tests begin with a trim flight, allowing the pilot to set control surface neutral locations, servo throw weights, and provide feedback on transmitter programming. Subsequent flights will be focused on isolating and verifying that the aircraft can complete more complex tasks, such as increased takeoff weight, payload functionality, and propulsion system performance. Final tests will consist of a complete competition run, including the ground mission and flight missions one through three.

8 Performance Results

8.1 Aerodynamics and Structures Performance Results

8.1.1 Wing Load Testing

The wing was loaded with sandbags at each station according to Table 22 in Section 7.1.1 beginning at a load factor equal to one. Each loading condition was allowed to settle for at least 30 seconds prior to measuring the deflection and increasing the load. The wing was loaded to a 5 g load condition equal to roughly 100 lbs. without failure. This loading condition simulates a 78.5-degree bank angle level turn taken at the target cruise speed of 85 mph. The maximum deflection versus load factor is provided in Figure 37 below.



Figure 36: Wing Loaded to $n = 5$ g.

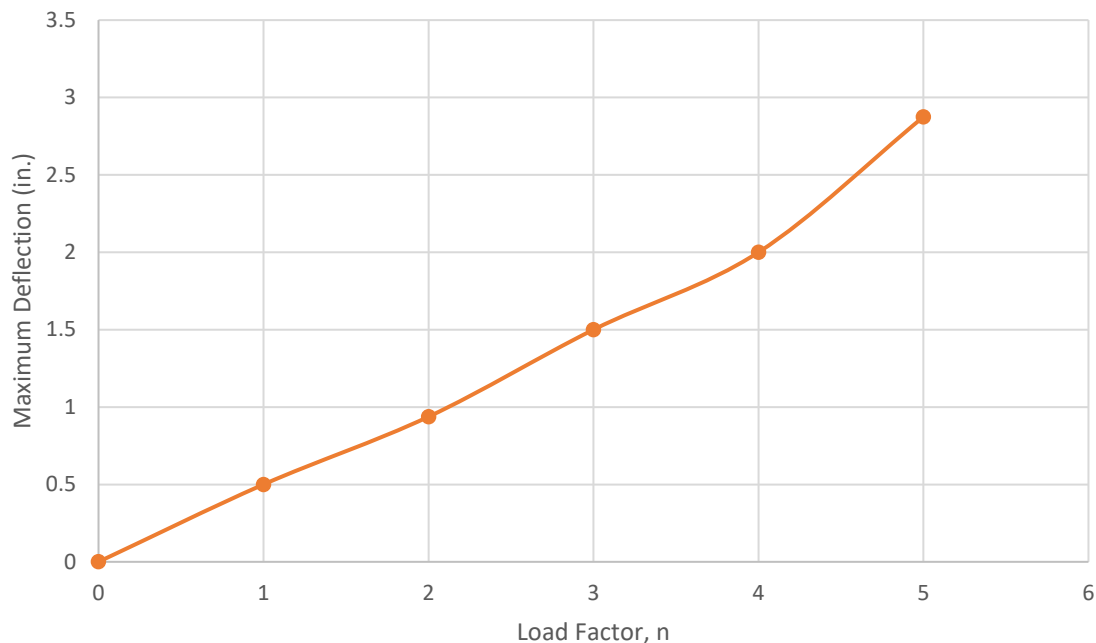


Figure 37: Wing load testing deflection results.



8.2.2 Wing Tip Testing

Prior to each flight during a flight test, the wing tip test is performed. The CG location was recorded at 33% of the chord in the early prototyping phase. In following flight tests, the center of gravity was recorded as 25% of the chord which was found to reduce elevator trim.

8.2 Payload Performance Results

8.2.1 Drop Testing

It was predicted that the sensor inside shipping container would survive a 30 in. drop on all six sides without damage to the sensor. Once the drop test was performed the sensor and shipping container structure were inspected for damage. During the test, the shipping containers were able to survive all the drop tests up to the 30 in. drop from all six sides with no damage to the shipping container and the sensor.

Table 24: Sensor Drop Testing Results.

| Sensor Drop Testing | | | |
|---------------------|------------------------|------------------------|--------------------------------|
| Drop Height(in) | 10 | 20 | 30 |
| Outcome | No damage on all sides | No damage on all sides | Fin delaminated on direct drop |

8.2.2 Wind Tunnel Testing

Based on calculations and testing, the sensor with a blunt nosecone will have enough drag to not swing forward during flight. The stability of the blunt sensor nosecone and the reliability of the alignment arm were validated using the wind tunnel for testing. The blunt nose cone was observed to provide enough drag to keep the sensor behind the aircraft while maintaining the aerodynamic stability of the sensor when deployed. From wind tunnel testing, the average retraction time was determined by filming the retraction of the sensor. The retraction rate averaged at 15.7 in./s which yields a retraction time for the 85 in. towline of approximately 5.5 s. During testing five successful retractions were recorded with only one retraction issue yielding an 83% success rate for the retractions. More testing is planned to mitigate the issues in alignment.

Table 25: Wind Tunnel Sensor Retraction Testing Results.

| Wind Tunnel Retraction Testing | | | | | | | |
|--------------------------------|---------|---------|---------|---------|----------------|---------|-------------|
| Retraction Trial | 1 | 2 | 3 | 4 | 5 | 6 | Overall |
| Outcome | Success | Success | Success | Success | Stuck on doors | Success | 83% Success |

8.3 Propulsion Performance Results

8.3.1 Battery Endurance During Static Thrust Testing

The battery capacity was tested on the static thrust stand configuration and was ran at a constant discharge rate of 40A. The voltage cutoff was set at 22.2V based on the 6-cell LiPo battery. The Figure 38 below shows that the motor was able to run for approximately 360 seconds. This was considered a passed test that validated the expected performance of a M_2 flight.

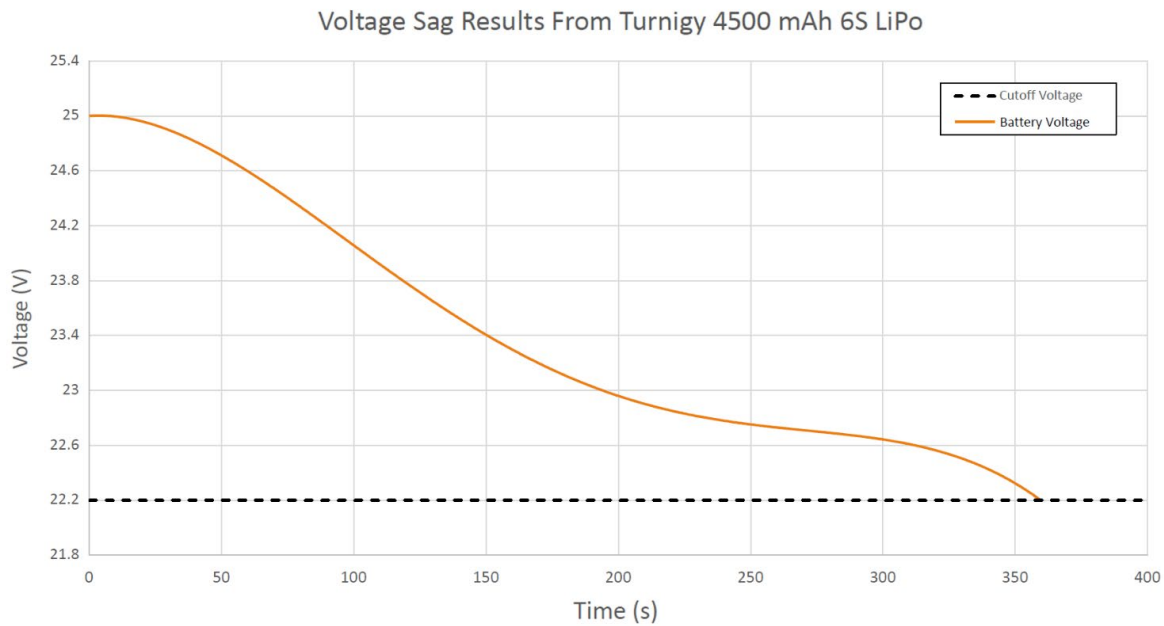


Figure 38: Battery Endurance Testing Results.

8.3.2 Propeller Optimization Testing

The thrust testing data shown in Figure 39 below determined that A 15x10 propeller would provide the greatest amount of thrust/current. The optimization testing also showed that the effects of propeller stall of increase significantly as the dimensions approach a square ratio, such as the 13.5x13.5.

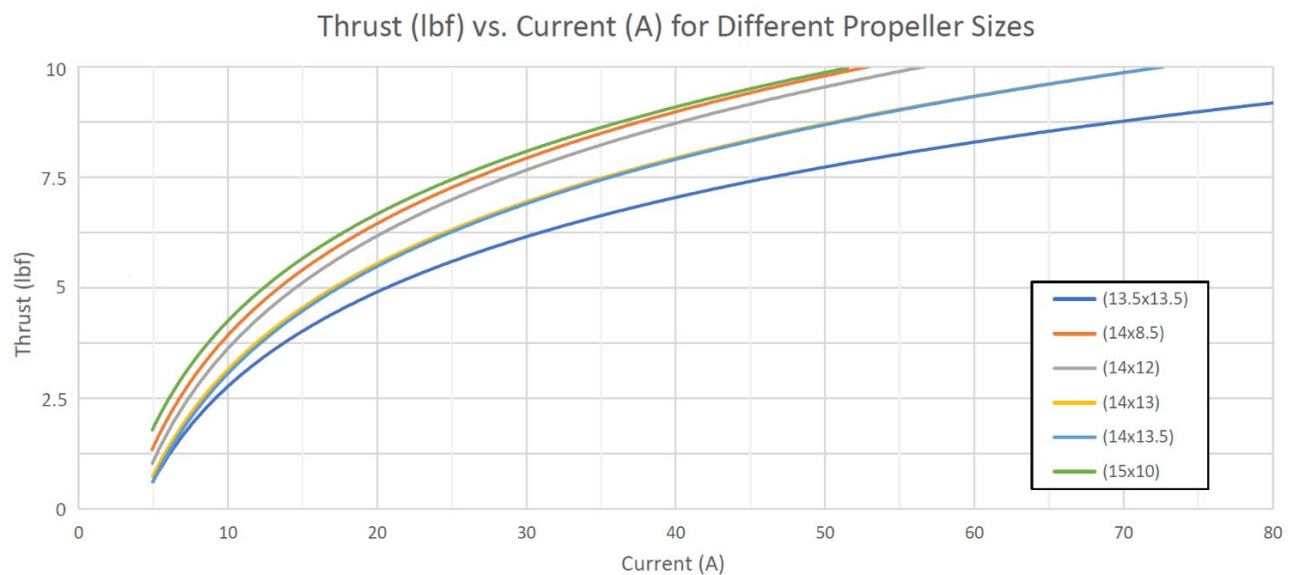


Figure 39: Thrust Vs Current of Different Propeller Dimensions on Static Thrust Stand.

8.3.2 Motor Thermal Evaluation

Estimates using the eCalc showed that the Turnigy SK3 motor had a critical temperature of 160 °F when combined with the 15x10 propeller. Historical temperature data collection from the National Weather Service



showed that Tucson, Arizona had the potential to reach a maximum temperature of 97 °F [7]. Extended testing of the propulsion system at an estimated 80% throttle was conducted in a room with equivalent temperatures to the Tucson climate. The FLIR image show in Figure 40 below shows that after a 12-minute test, the motor reached a temperature of 106.7 °F, well under the thermal limit in static configuration. During a competition flight, the convective heat transfer would allow the motor to operate at safe temperature, increasing thrust output and motor efficiency.

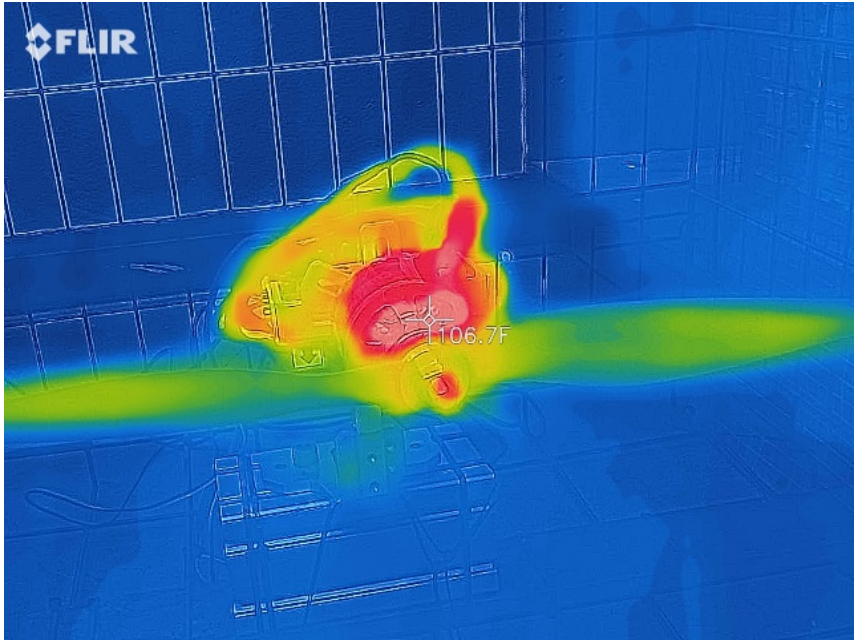


Figure 40: FLIR Image of Turnigy Motor After 12-Minute Thermal Stress Test.

8.3.3 Flight Performance

Estimated and actual mission flight speeds were compared side by side by using both eCalc simulations and actual flight test data in Table 26 below. From the estimated values, it is expected for the aircraft to cruise at 130 ft/s for Missions 1 and 3 and 100 ft/s for Mission 2.

Table 26: Predicted Versus Actual Flight Performance During Flight Testing.

| Flight Mission | Parameter | Predicted Value | Actual Value | Δ% |
|----------------|--------------|-----------------|--------------|--------|
| Mission 1 | Cruise Speed | 134.9 ft/s | 121.7 ft/s | -10.8% |
| | Current Draw | 102.8 A | TBD | TBD |
| Mission 2 | Cruise Speed | 105.3 ft/s | TBD | TBD |
| | Current Draw | 114 A | TBD | TBD |
| Mission 3 | Cruise Speed | 124.1 ft/s | TBD | TBD |
| | Current Draw | 100.2 A | TBD | TBD |

In Flight Test 2, the aircraft successfully logged flight speed data for Mission 1 with the aid an Eagle Tree telemetry system. The recorded cruise speed was just under the predicted cruise speed by 10.8% In future flight tests, current draw from each motor will be collected in addition to cruise speeds.



8.4 Flight Testing Outcomes

Flight Test 1 11/01/2020:

Results

- Five successful flights were flown, validating aircraft's flight characteristics and flying with increased weight.

Improvements

- From observed and recorded data, the aerostructures team will double the chord of the elevator in order to provide better aerodynamic stability and a stronger elevator pitch force.
- A steerable rudder will be added, and the propulsion team will remove differential thrust in order to make yaw control easier and more intuitive for the pilot.
- The landing gear will be reinforced for strength and a servo will be added to the front landing gear to allow better yaw control while taxiing.
- The flaperon wing configuration will be replaced with separate flaps and ailerons to increase aircraft stability during aircraft landings and takeoffs.

Flight Test 2 11/15/2020:

Results

- Two total flights flown with one successful flight, testing optimized aircraft and payload module functionality.
- Due to accidental signal wire short, right motor was reprogrammed, resulting in air brake during first flight upon reaching maximum throttle.

Improvements

- The propulsion sub team will program out the motor breaking feature of the ESC's.
- Aileron throw will be reduced by 25% on the transmitter. By the pilot's request, ailerons, elevator, and rudder will have exponential throw on the transmitter. The payload team will adjust the design of the payload doors to allow the sensor to deploy faster.

Flight Test 3 01/09/2021

Results

- Three total flights flown, with one crash.
- Upgraded payload module and the aircraft's performance at MTOW.
- Crash occurred during mission 2 simulation when loaded up with 17.6 lb. or 94% of predicted MTOW

Improvements

- The payload team will switch the tow line's material from fishing line to Kevlar to reduce elastic bouncing while deployed.
- Landing gear material to be changed to steel in order to prevent bending during landing for weighted flights.



- Mounting plate attaching wing to fuselage will be redesigned in order to minimize the stress concentration that resulted in a crash during flight three.
- A new fuselage will be manufactured with fiberglass instead of foam to increase structural strength and move towards a competition ready aircraft.



Figure 41: Flight Path of Aircraft Recorded During A M_1 Simulation.

Flight Test 4 Outcomes:

Results

- No flights completed.
- Runway taxi test completed as the aircraft was deemed too heavy to fly.

Improvements

- The fuselage will be remanufactured with fewer plies to reduce weight, and special consideration will be taken in ensuring the CG location of the fuselage meshes with that of the landing gear and wing.



Figure 42: First Composite Fuselage Aircraft Prototype.



9 Bibliography – All

- [1] ANSI/AIAA, 1992, "Recommended Practice for Atmospheric and Space Flight Vehicle Coordinate Systems," Washington, D.C.
- [2] Lyon, C.A., et al., 1997, "Summary of Low-Speed Airfoil Data," SoarTech Publications, Virginia Beach, VA.
- [3] Gudmundsson, S., 2014, General Aviation Aircraft Design: Applied Methods and Procedures, Elsevier Butterworth-Heinemann, Oxford, UK.
- [4] Raymer, D.P., 1992, Aircraft Design: A Conceptual Approach, American Institute of Aeronautics and Astronautics, Washington, D.C.
- [5] Hoerner, S.F., 1965, Fluid Dynamic Drag, Liselotte A. Hoerner, Great Britain.
- [6] Schrenk, O., 1941, "A Simple Approximation Method for Obtaining the Spanwise Lift Distribution," The Journal of the Royal Aeronautical Society, 45(370), pp. 331-336.
- [7] National Weather Service Corporate Image Web Team, 2005, "NWS Tucson," National Weather Service.